Redox Biology 77 (2024) 103368

Contents lists available at ScienceDirect

Redox Biology

journal homepage: www.elsevier.com/locate/redox

Unraveling the nexus of oxidative stress, ocular diseases, and small extracellular vesicles to identify novel glaucoma biomarkers through in-depth proteomics

Raquel Rejas-González [a,b], Ana Montero-Calle [a,1], Natalia Pastora Salvador [c], María José Crespo Carballés [c], Emma Ausín-González [c], Juan Sánchez-Naves [d], Sara Pardo Calderón [a,b], Rodrigo Barderas [a,e,**,1], Ana Guzman-Aranguez [b,*,1]

[a] Chronic Disease Programme, UFIEC, Instituto de Salud Carlos III, 28220, Majadahonda, Madrid, Spain
[b] Biochemistry and Molecular Biology Department, Facultad de Óptica y Optometría, Universidad Complutense de Madrid, 28037, Madrid, Spain
[c] Opthalmology Service, Hospital Universitario Infanta Leonor, 28031, Madrid, Spain
[d] Oftalmedic Salvà, 07013, Palma, Illes Balears, Spain
[e] CIBER of Frailty and Healthy Aging (CIBERFES), 28029, Madrid, Spain

ARTICLE INFO

Keywords:
Glaucoma
Cataracts
Small extracellular vesicles
Proteomics
Aqueous humor
Glaucoma diagnosis

ABSTRACT

Chronic ocular pathologies such as cataracts and glaucoma are emerging as an important problem for public health due to the changes in lifestyle and longevity. These age-related ocular diseases are largely mediated by oxidative stress. Small extracellular vesicles (sEVs) are involved in cell-to-cell communication and transport. There is an increasing interest about the function of small extracellular vesicles (sEVs) in the eye. However, the proteome content and characterization of sEVs released by ocular cells under pathological conditions are not yet well known. Here, we aimed to analyze the protein profile of sEVs and the intracellular protein content from two ocular cell lines (lens epithelial cells and retinal ganglion cells) exposed to oxidative stress to identify altered proteins that could serve as potential diagnostic biomarkers. The protein content was analyzed by quantitative mass spectrometry-based proteomics. Validation was performed by WB and ELISA using cell extracts and aqueous humor from cataract and glaucoma patients. After data analysis, 176 and 7 dysregulated proteins with an expression ratio≥1.5 were identified in lens epithelial cells' protein extract and sEVs, respectively, upon oxidative stress induction. In retinal ganglion cells, oxidative stress induction resulted in the dysregulation of 1033 proteins in cell extracts and 9 proteins in sEVs. In addition, by WB and ELISA, the dysregulation of proteins was mostly confirmed in aqueous humor samples from cataract or glaucoma patients in comparison to ICL individuals, with RAD23B showing high glaucoma diagnostic ability. Importantly, this work expands the knowledge of the proteome characterization of cataracts and glaucoma and provides new potential diagnostic glaucoma biomarkers.

1. Introduction

Chronic ocular diseases represent a burgeoning public health challenge fueled by the demographic aging and evolving lifestyles. It has been estimated that 95 and 80 million people worldwide are affected by cataracts [1] and glaucoma [2], respectively.

Abbreviations: sEVs, small extracellular vesicles; IOP, intraocular pressure; ROS, reactive oxygen species; H_2O_2, hydrogen peroxide; HLE-B3, human lens epithelial cells; R28, rat retinal ganglion cells; ICL, implantable collamer lens; TMT, Tandem Mass Tag; WB, western blot; H_2Omq, H_2O Milli-Q; AUC, area under the curve; LC-MS/MS, liquid chromatography tandem mass spectrometry; TEM, transmission electron microscopy; TFA, trifluoracetic acid; FA, formic acid; ACN, acetonitrile; O/N, overnight; RT, room temperature; PCA, principal component analysis; AGC, automatic gain control; IT, injection time; PIF, precursor intensity fraction; FDR, false discovery rate; SL, sample loading; TMM, trimmed mean of M-values; MCL, Markov cluster algorithm; RAD23B, UV excision repair protein RAD23 homolog B.

* Corresponding author. Biochemistry and Molecular Biology Department, Universidad Complutense de Madrid, E-28037, Madrid, Spain.
** Corresponding author. Functional Proteomics Unit, UFIEC, Instituto de Salud Carlos III, E-28220, Majadahonda, Madrid, Spain.
E-mail addresses: r.barderasm@isciii.es (R. Barderas), aguzman@ucm.es (A. Guzman-Aranguez).
[1] Co-senior authors.

https://doi.org/10.1016/j.redox.2024.103368
Received 1 August 2024; Received in revised form 4 September 2024; Accepted 20 September 2024
Available online 21 September 2024

Oxidative stress is a key factor in the development of both pathologies. Ocular tissues are continually exposed to visible light and UV radiation throughout life, such exposure leads to the photochemical generation of free radicals, especially reactive oxygen species (ROS) such as hydrogen peroxide (H_2O_2) or the superoxide radical. At endogenous level, mitochondria are the main source of ROS in the eye. During the aging process, an imbalance can occur between ROS and antioxidant defenses, increasing ROS levels [3] and leading to oxidative stress. Lens epithelial cells are the first barrier against potentially harmful external factors, and their sensitivity to oxidative damage is a major contributor to cataractogenesis. The progressive accumulation of oxidative damage with aging can exceed the antioxidant capacity of the lens, leading to lipid peroxidation, crystalline aggregation, DNA damage, and subsequent apoptosis and pyroptosis of lens epithelial cells [4–6]. Previous studies in the literature reported elevated concentration of H_2O_2 in lens and aqueous humor samples from cataract's patients as compared to control subjects [7]. Furthermore, it has been described that lens, in organ culture, develop cataracts when they are incubated with increased H_2O_2 levels [8].

Glaucoma is characterized by retinal ganglion cell death and the progressive and irreversible degeneration of the optic nerve. High intraocular pressure (IOP) is a proven risk factor of glaucoma and pharmacological treatment is mainly based on IOP reduction. Moreover, several concomitant factors such as increased ROS production and oxidative retina damage have been postulated as the crucial factors in early retinal injury [9]. Altered redox status have been assessed in serum and aqueous humor of glaucoma patients, showing a general elevation in oxidative stress markers [10,11].

Increased ROS levels in the aqueous humor can produce alterations in the trabecular meshwork [12] causing trabecular thickening and affecting trabecular meshwork cell survival [13]. These changes in trabecular meshwork increase resistance to aqueous humor drainage, leading to increased IOP. Elevated IOP can damage mitochondria [14] and mitochondrial dysfunction favors ROS production and oxidative retinal damage. ROS can constitute a direct cytotoxic stimulus, causing retinal ganglion cell loss in a caspase-dependent and independent manner [15]. In addition, oxidative stress can induce other intracellular pathways leading to retinal ganglion cell death. Oxidative stress modifies the glutamate/glutamine cycling inducing extracellular neurotoxic glutamate increase [16,17]. Furthermore, oxidative stress also represents a main route for mitochondria-originated inflammatory responses resulting in glial neuroinflammation processes and inflammatory cytokines production [18]. Oxidized mtDNA can activate inflammasomes [19] resulting in pyroptosis (inflammatory cell death) of retinal ganglion cells in glaucoma [20]. Additional evidence supports the role of oxidative stress-related in autophagy induction and retinal ganglion cells loss can also be due to altered autophagic process [12].

Recent studies have revealed that exposure to oxidative stress can modify the secretory activity and small extracellular vesicles (sEVs) release by some ocular cells. sEVs have emerged as key players in the intricate landscape of intercellular communication [21]. The ability of sEVs to shuttle molecular information between cells indicate their involvement in physiological processes and pathological conditions, although information about their relationship with ocular diseases is still limited. The presence of exosomes has been detected in ocular biological fluids such as tear fluid [22], aqueous humor [23], and vitreous humor [24]. Moreover, under oxidative stress conditions, an increase in sEVs release from retinal pigment epithelial cells [25], as well as changes in their content, have been determined [26,27]. Furthemore, sEVs derived from lens epithelial cells exposed to different oxidative stress factors (hydrogen peroxide and UV) altered the behavior of lens epithelial cells [28,29] and induced epithelial-mesenchymal transition in mouse lenses, promoting opacification of the posterior capsule [29]. Considering the potential involvement of sEVs in the pathogenesis of several ocular diseases, including cataract and glaucoma, modifications of sEVs cargo could reflect changes of ocular diseases. However, despite the importance of oxidative stress in cataract and glaucoma development and glaucomatous neurodegeneration, few studies have analyzed in-depth changes in the intracellular proteome and in the sEVs protein content of lens epithelial cells and retinal ganglion cells after exposure to oxidative stress. This analysis could facilitate the elucidation of unknown molecular pathological mechanisms, the identification of new diagnostic biomarkers, and the determination of potential therapeutic targets. In this work, we have identified and validated changes in the intracellular protein content as well as in the protein cargo of sEVs from lens epithelial cells and retinal ganglion cells exposed to oxidative stress. Our results indicate that the quantitative characterization of the intracellular proteins and the sEVs protein content released from ocular cells exposed to relevant oxidative stress conditions is useful to delve deeper into the protein expression changes produced by oxidative stress and allow identifying potential diagnostics biomarkers in the development of eye diseases. Particularly, we have revealed the diagnostic potential of one of the dysregulated proteins identified (RAD23B) to discriminate glaucoma patients from cataracts patients and ICL (implantable collamer lens) individuals, which were used as controls in the study, through the analysis of aqueous humors by ELISA.

2. Material and methods

2.1. Cell lines

Human HLE-B3 cells (ATCC®, VI, USA) and rat R28 cells (Kerafast, MA, USA) were used in the study. HLE-B3 cells were grown in Minimum Essential Medium (M560, Merck, Germany) supplemented with 20 % Fetal Bovine Serum, 0.5 % penicillin/streptomycin, 1 % sodium pyruvate (100 mM), and 1 % MEM non-essential amino acids (all from Thermo Fisher Scientific, MA, USA). R28 cells (Kerafast) were grown in Dulbecco's Modified Eagle's Medium (D5523, Merck) supplemented with 3 % sodium bicarbonate (Merck), 10 % calf serum (Thermo Fisher Scientific), 1 % MEM non-essential amino acids (Thermo Fisher Scientific), 1 % MEM vitamins (Merck), 1 % L-glutamine (Merck), and gentamicin (10 μg/ml, Thermo Fisher Scientific). To induce oxidative stress, HLE-B3 and R28 cell lines were incubated for 24 h with 350 μM and 600 μM H_2O_2, respectively, in their cell culture medium and compared with the same cells incubated without H_2O_2 as controls of the assays.

2.2. Aqueous humor samples

The clinical and ethical aspects of this study were approved by the Ethical Committee of Hospital Universitario Infanta Leonor (Madrid, Spain) (CEIC 011–23, February 2, 2023) and Ophthalmedic and I.P.O. Institute (Palma de Mallorca, Spain). All patients provided written informed consent for the use of their biological samples for research purposes, adhering to ethical principles outlined by Spain (LOPD 15/1999) and the European Union Fundamental Rights of the EU (2000/C364/01). Patient data were processed in accordance with the Declaration of Helsinki (last revision 2013) and the Spanish National Biomedical Research Law (14/2007, of 3 July). Aqueous humor was extracted at the beginning of surgery using 2 % lidocaine anesthetic drops. A 30-gauge Rycroft cannula on a tuberculin syringe (1 mL) was utilized to aspirate the aqueous humor. Extraction was performed using a clear corneal microincision under surgical microscope vision, moving the cannula parallel to the limbus from the periphery to the center of the eye's anterior chamber. Aqueous humor (0.3–0.4 mL) was collected per patient and stored immediately after surgery at −20 °C and subsequently at −80 °C. The study included aqueous humor samples from three different groups: ICL (implantable collamer lens) individuals, and cataract, and glaucoma patients (Table 1 and Supplementary Table 1). The ICL group comprised individuals with a transparent lens (without cataracts) undergoing refractive surgery with the inclusion of an intraocular lens. The cataract group included patients referred for cataract

Table 1
Clinicopathological characteristics of the patients involved in the study.

Samples		Number (n)	Age average ± SD (years)	Min. Age (years)	Max. Age (years)	Gender (n)	
						M	F
WB	**ICL**	4	47.5 ± 14.43	26	57	1	3
	Cataracts	5	68.6 ± 7.73	60	79	3	2
	Glaucoma	5	66.4 ± 12.66	51	80	1	4
	Pool ICL	4	45.25 ± 12.34	31	57	1	3
	Pool cataracts	5	73.6 ± 14.10	55	89	2	3
	Pool glaucoma	4	62.25 ± 11.00	55	74	1	3
ELISA	**ICL**	28	42.6 ± 12.19	22	59	8	23
	Cataracts	28	68.4 ± 10.17	49	91	17	17
	Glaucoma	24	70.79 ± 12.99	26	89	11	18

surgery without glaucoma and with non-diabetic cataracts. The glaucoma group consisted of aqueous humor samples from glaucoma patients referred for cataract surgery. Individuals with other ophthalmological diseases were excluded. Pooled aqueous humor samples were used for proteomics analysis, while both pooled and individual samples were used for validation (Table 1 and Supplementary Table 1).

2.3. Small extracellular vesicles (sEVs) isolation, purification, and characterization

sEVs were isolated and purified from 120 mL of conditioned medium of cell lines by ultracentrifugation, according to established protocols [30,31]. sEVs pellets were resuspended in PBS 1X and stored at −80 °C until use.

Prior to further use, sEVs were characterized by NanoSight-Nanoparticle Tracking Analysis (NTA) and transmission electron microscopy (TEM), as previously described [30,31]. For NanoSight analyses, a 1:100 dilution of purified sEVs in PBS 1X was prepared and analyzed with a NanoSight NS3000 (Malvern Panalytical, United Kingdom). Two different sEVs isolations were analyzed in the NanoSight and three acquisitions of 60 s (infusion rate of 70 μL/min) from each sample measured. For the analysis, the mean and standard deviation of the three acquisitions for the two isolations was represented with GraphPad Prism 8. For TEM, sEVs isolated from 120 mL of conditioned medium were fixed, negatively stained, and analyzed using an FEI Tecnai 12 electron microscope.

2.4. Cell protein extraction and quantification

Cell lines were grown until 90 % confluence at 37 °C and under 5 % CO_2 and harvested with PBS 1X containing 4 mM EDTA (ethylenediaminetetraacetic acid). Cells were then collected by centrifugation at 1200 rpm for 5 min and room temperature (RT), and the supernatant was discarded. Cell pellet was resuspended in lysis buffer (RIPA) supplemented with 1:100 diluted phosphatase and protease inhibitors (MedChemExpress, USA) and lysed by mechanical disaggregation using needle syringes. Finally, samples were clarified by centrifugation at 10000×*g* for 15 min and the supernatants (protein extracts) stored at −80 °C until use. Protein concentration was determined using the commercial BCA Protein Assay Kit (Thermo Fisher Scientific) and verified by Western blot, and Coomassie blue and silver staining after 10 % PAGE-SDS electrophoresis.

2.5. Mass spectrometry

For the quantitative proteomics analysis, R28 cell and sEVs protein extracts were used in triplicate, whereas HLE-B3 cell and sEVs protein extracts were used in duplicate. 5 μg of each sEVs protein extract, or, alternatively, 10 μg of each cell protein extract in a final volume of 100 μl with RIPA buffer, were analyzed according to established protocols [31–34]. For the sEVs, samples were incubated with the RIPA buffer 5 min at 95 °C and 5 min on ice (3 times) to improve the release of sEVs proteins. Each sEVs and cell extract sample was separately reduced with 10 μL 100 mM TCEP for 45 min, 37 °C, and 600 rpm. Then, samples were alkylated with chloroacetamide (40 mM final concentration) for 35 min at RT, in darkness, and 600 rpm. Then, samples were incubated 30 min at RT with 200 μl of 100 % acetonitrile (ACN) and 5 μl of SeraMag magnetic beads mix (50 % hydrophilic beads - 50 % hydrophobic beads, GE Healthcare) per sample. Magnetic beads with proteins anchored were washed twice with 70 % ethanol and once with ACN. Supernatants were discarded and proteins were digested overnight (O/N) at 37 °C and 600 rpm with porcine trypsin (Thermo Fisher Scientific) in a 1:20 (trypsin:protein) relation, in 100 μL of 200 mM HEPES, pH 8. Supernatants were collected after 2 min sonication, and each sample was then separately labeled with a different Tandem Mass Tags (TMT) 10-plex reagent (Thermo Fisher Scientific). Labeling consisted of two incubation steps of 30 min at RT and 600 rpm with 10 μL of the corresponding TMT reagent per incubation, and a final incubation with 10 μL of 1 M glycine, pH 2.5 for 30 min at RT and 600 rpm. Finally, samples were dried under vacuum and reconstituted in 300 μL of 0.1 % Trifluoracetic acid (TFA) in H_2Omq before peptide separation using High pH Reversed-Phase Peptide Fractionation Kit (Thermo Fisher Scientific). First, columns were equilibrated twice with 300 μL of ACN and twice with 300 μL of 0.1 % TFA in H_2Omq. After loading the peptides, columns were washed twice with 300 μL of 0.1 % TFA in H_2Omq, and peptides were separated in 12 fractions of 300 μL in 0.1 % triethylamine and increasing amounts of ACN (2.5–100 %). Finally, fractions were dried under vacuum and stored at −80 °C until use. Samples were reconstituted in 10 μL of 0.1 % Formic acid (FA) prior to LC-MS/MS analysis.

TMT experiments of sEVs and cell protein extracts were analyzed onto an Orbitrap Exploris 480 mass spectrometer (Thermo Fisher Scientific) equipped with FAIMS Pro Duo interface technology. The Vanquish Neo UHPLC System (Thermo Fisher Scientific) was used for peptide separation. Each fraction was loaded into a precolumn PepMap 100C18 3 μm, 75 μm × 2 cm Nanoviper Trap 1200BA (Thermo Fisher Scientific) and eluted in an Easy-Spray PepMap RSLC C18 2 μm, 75 μm × 50 cm (Thermo Fisher Scientific) heated at 50 °C. The mobile phase flow rate was 300 nL/min and elution buffers composition were 0.1 % FA in H_2Omq (Buffer A) and 0.1 % FA in 80 % ACN (Buffer B). Buffers were used in an elution gradient of 2 h: 0%–2% buffer B for 4 min, 2 % buffer B for 2 min, 2%–42 % buffer B for 100 min, 42%–72 % buffer B for 14 min, 72%–95 % buffer B for 5 min, and 95 % buffer B for 10 min. For the sEVs analysis, 6 μL (fractions 1 to 4) or 8 μL (fractions 5 to 12) of each sample were injected into the mass spectrometer. For the cell extracts experiment, 4 μL (fraction 1) or 6 μL (fractions 2 to 12) of each sample were injected into the mass spectrometer. Ionization was performed with a liquid junction voltage of 1900 V and a capillary temperature of 280 °C. Full scan method consisted of a *m/z* of 350–1400, an Orbitrap resolution of 60000 (at *m/z* 200), an automatic gain control (AGC) value of 300 %, and maximum injection time (IT) of 25 ms. For MS/MS fragmentation, the 12 more intense precursor ions detected in the survey scan were selected. Normalized collision energy used for the fragmentation was 34 and MS/MS scans were acquired with 100 *m/z* first mass, 100 % of AGC, resolution of 15000 (at *m/z* 200), intensity

threshold of $2x10^4$, isolation window of 0.7 *m/z* units, a maximum IT of 22 ms, and the TurboTMT enabled. Unassigned, singly charged, and greater than or equal to seven protonated ions were rejected during the charge state screening. The dynamic exclusion time selected to discriminate against previously selected ions was 45 s. For FAIMS, a gas flow of 4 L/min and CVs −60V and −45V were used.

2.6. Data analysis

MS data analysis was performed with MaxQuant (version 2.1.3). Mass spectra files were searched against the Uniprot UP000005640_9606.fasta *Homo sapiens* (human) 2022 database (20577 entries, downloaded: March 2022) and the UP000002494_10116 Rattus Norvegicus (rat) 2022 database (46595 entries, downloaded: December 2022). Precursor mass tolerance was set to 4.5 ppm and reporter mass tolerance to 0.003 Da allowing up to two missed cleavages. Carbamidomethylation of cysteines was set as fixed modification and methionine oxidation. N-terminal acetylation, and Ser, Thr, and Tyr phosphorylation were set as variable modifications. Both unique and razor peptides with a minimal length of 7 amino acids and a maximal mass of 4600 Da were considered for quantification. Identified peptides were filtered by their precursor intensity fraction (PIF) with a false discovery rate (FDR) threshold of 0.01. Proteins identified as potential contaminants were excluded, whereas proteins with an ion score over 99 % and with at least one unique peptide were selected for further analysis. The estimation of the sequence coverage for specific proteins was calculated with the percentage of matching amino acids from the identified peptides having confidence greater than or equal to 95 % divided by the total number of amino acids in the sequence. To avoid interference due to overlapping, reporter ion intensities were corrected according to manufacturer's data sheet.

Moderated t-statistics analyses were performed with R Studio (version 4.1.1) and the packages "dplyr", "tidyverse", and "limma", following previously described protocols (https://pwilmart.github.io/TMT_analysis_examples/KUR1502_PAW_limma.html, accessed July 2022). The moderated t-statistics was applied to identify differentially expressed proteins of high-throughput biological data in this proteomics experiment with small sample sizes. Specifically, the "limma" package employed here uses an empirical Bayes method to moderate the protein-wise sample variances towards a common value, which was calculated using a posterior variance estimator that combines the protein-specific sample variances with information borrowed from the ensemble of all proteins. Additionally, the R package "ggplot2" was used for data visualization. First, TMT experiment normalization was performed to equal the differences in the total sum of signals of each TMT channel, as the same amount of protein was labeled in each TMT sample. Sample loading (SL) and Trimmed Mean of M-values (TMM) data normalization was performed following established protocol with R Studio (version 4.1.1), using "tidyverse", "psych", "gridExtra", "scales", and "ggplot2" packages. To determine sample clustering, principal component analysis (PCA) was performed with "stats" R package. Prior to statistical analysis, contaminants and reverse proteins were removed, data was filtered (proteins identified in at least 50 % of samples were considered for the analysis), and missing values imputation by random draws from a gaussian was performed using the "imputeLCMD" R package. After the statistical analysis, proteins selected as statistically significant dysregulated were the ones identified with at least one unique peptide and an expression ratio $\geq$1.5 or $\leq$0.67 and p-value $\leq$0.05. Bioinformatics analyses of the proteins identified as dysregulated were subsequently performed with STRING (version 12.0) and the R packages "STRINGdb" (version = 11.5) and "ReactomePA" to identify the altered networks and pathways in which these proteins are involved. For protein interaction networks, STRING settings were fixed to MCL clustering enrichment 2 and 0.4 confidence score. For the enrichment pathway analysis, the most significantly enriched cellular components or biological processes with a false discovery rate (FDR) lower than 0.05 in which these dysregulated proteins are involved were represented.

2.7. SDS-PAGE and Western blot

Protein expression of proteomics samples was analyzed by Coomassie blue staining and Western blot (WB). 5 μg of sEVs an, alternatively, 5–40 μg of cell protein extracts depending on the protein analyzed were loaded into a 10 % SDS-PAGE under reduced conditions. For the analysis of aqueous humors samples for validation, 5 μg of individual (ICL N = 4, Cataracts N = 5, and Glaucoma N = 5) or pooled (ICL N = 4, Cataracts N = 5, and Glaucoma N = 4) samples were used. After SDS-PAGE, proteins were transferred to nitrocellulose membranes that were incubated with the corresponding primary and secondary antibodies (Supplementary Table 2), according to established protocols [32,35]. ECL Pico Plus chemiluminescent reagent (Thermo Fisher Scientific) was used for signal development, and an Amersham ImageQuant 800 GxP biomolecular imager (Cytiva, USA) to detect the signal and obtain the images. Image J software was used for the quantification of protein band intensities, and GAPDH protein intensity was used as loading control and for normalization.

2.8. ELISA tests

ELISA tests were performed to quantify the expression of RAD23B (orb441875, Biorbyt, USA) in aqueous humor from ICL (N = 28), and patients with cataracts (N = 28) or with cataracts and glaucoma (N = 24), according to the manufacturer's instructions. Aqueous humor samples were used at a 1:10 dilution. Protein concentration was determined after optical density measurement of each well at 450 nm in The Spark multimode microplate reader (Tecan Trading AG, Switzerland). ROC curves and Mann-Whitney U tests were obtained to determine the significance of the results.

2.9. Statistical analyses

The statistical analyses of Western blot (Welch t-tests) data were performed using Microsoft Excel, and the statistical analysis of the ELISA data, which included Mann-Whitney U tests and ROC curves, were performed using R Studio (version 4.1.1) and the R packages "ModelGood", "Epi", and "pROC". A p-value lower than 0.05 was considered statistically significant.

3. Results

In this work, TMT quantitative proteomics was used to identify dysregulated proteins associated with eye pathological conditions characterized by extensive oxidative stress: cataracts and glaucoma. Oxidative stress was induced upon H_2O_2 exposure in two different cell lines as models of cataracts (human lens epithelial cells, HLE-B3) and glaucoma (rat retinal ganglion cells, R28). Then, their proteome and the sEVs proteome were analyzed by proteomics (*see* Graphical Abstract for a schematic view of the workflow), and dysregulated proteins associated to each pathology identified. For validation, cell extracts and aqueous humors samples were analyzed by WB and ELISA.

3.1. Isolation and characterization of sEVs from cells exposed to oxidative stress

Prior to proteomics analysis, the quality of the sEVs isolated by ultracentrifugation from serum-free conditioned medium of ocular cell lines was analyzed by NanoSight NS3000 and TEM. By NanoSight, it was observed a multimodal distribution with the presence of heterogeneous sEVs in size, where the predominant sEVs sizes in all samples were smaller than 200 nm, ranging between 50 and 200 nm (Fig. 1A). In some replicates, sEVs with a larger size (>400 nm) were observed. It was previously observed that isolated vesicles can undergo aggregation [36].

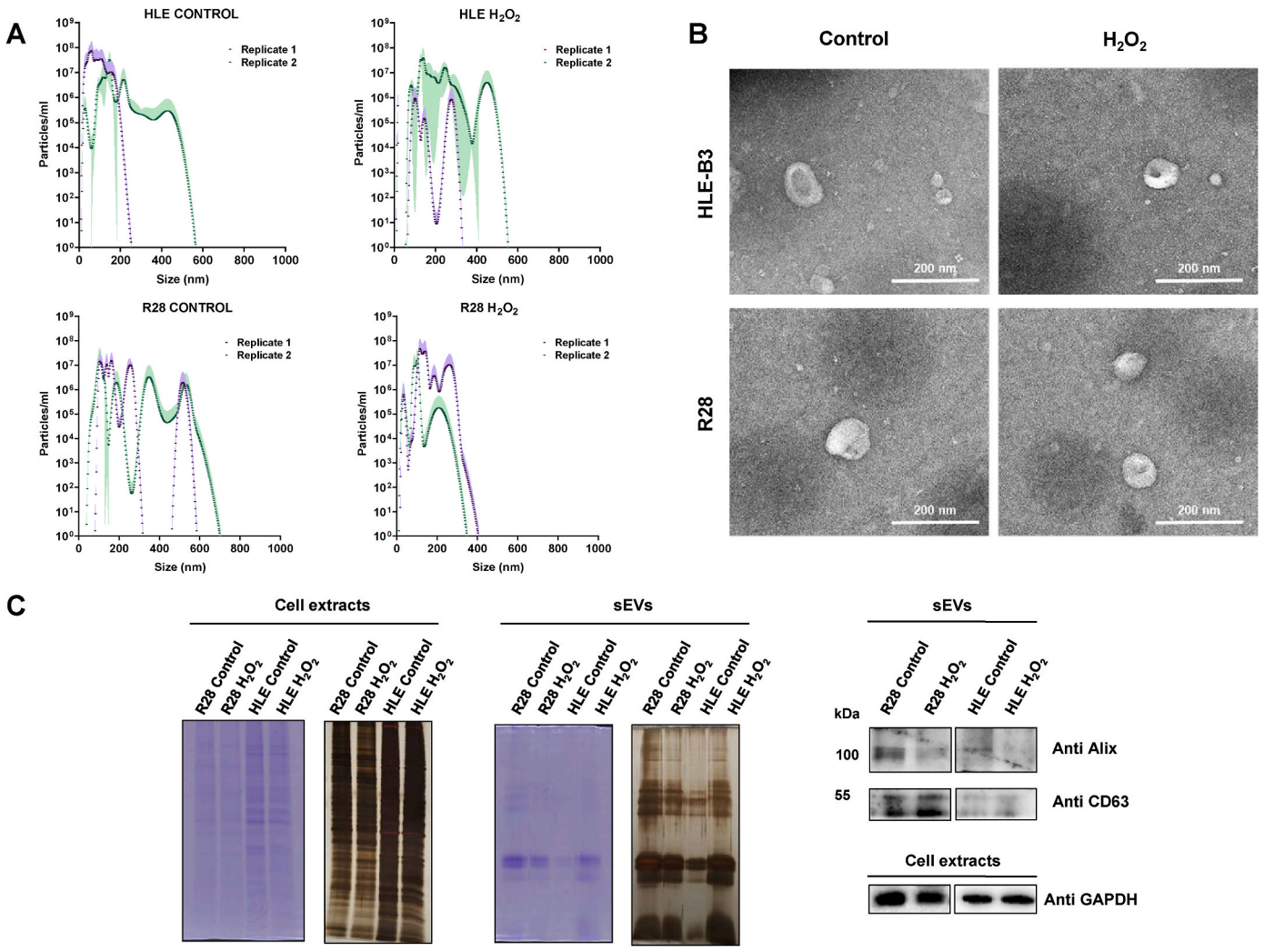

Fig. 1. Verification of the quality of sEVs isolated from ocular cell lines. Nanosight (A), TEM (B), and Coomassie blue and silver staining and WB (C) confirmed the compatibility of the isolated vesicles with sEVs in terms of size, morphology, and protein content. Log scale was used in (A) to represent particles/ml. (For interpretation of the references to colour in this figure legend, the reader is referred to the Web version of this article.)

Since the particle size is inferred from the diffusion constant of the Brownian motion in nanoparticle tracking analysis, the presence of possible aggregates could lead to a decreased diffusion constant and a consequent increase in the nanoparticle tracking analysis particle size estimation [37]. Moreover, in HLE-B3, the exposure to H_2O_2 cells induced a wider size distribution detecting a shift toward larger sizes. In contrast, in R28 cells exposed to H_2O_2, the main size distribution of sEVs remained within a narrow range (Fig. 1A). Additionally, this effect was also accompanied of a slight decrease in particle concentration after H_2O_2 in both cell lines.

Additionally, we confirmed an appropriate isolation of the sEVs by TEM, where the size and morphology of the vesicles was compatible with sEVs (Fig. 1B). Finally, the different protein content of the cell extracts and the extracellular vesicles as observed by SDS-PAGE and Coomassie Blue and silver staining, together with the immunostaining with specific sEVs markers CD63 and Alix, confirmed the correct isolation of the sEVs derived from the conditioned medium of the cells (Fig. 1C). Then, we proceed to the proteomics analyses of the sEVs protein content upon oxidative stress induction as well as cell extracts analysis.

3.2. Identification of dysregulated proteins from sEVs and cell extracts

To identify dysregulated proteins in cataracts and glaucoma pathologies, two TMT 10-plex experiments were performed for the proteomics characterization of sEVs and cell extracts samples from HLE-B3 and R28 control and H_2O_2 cell lines and analyzed using an Orbitrap Exploris 480 equipped with FAIMS Pro Duo Interface. Subsequent protein identification and quantification, and differential expression analysis was performed with the MaxQuant and R software, respectively.

Prior to the analysis to survey for dysregulated proteins in sEVs or cell extracts upon oxidative stress induction, the clustering of the samples by PCA analysis was studied (Fig. 2). Separated clusters for control and H_2O_2 samples were observed in all experimental samples. Importantly, all samples were used for the identification of dysregulated proteins under oxidative stress conditions, but R28_H_2O_2_3 replicate sample from the R28 sEVs, which was omitted in the analysis because it did not cluster together its corresponding replicates (Fig. 2A).

After data normalization (Supplementary Fig. 1), 32 and 4821 proteins were identified and quantified with at least one unique peptide and an ion score above 99 % in sEVs and cell extracts of R28 cell line respectively, whereas for the HLE-B3 cells 55 and 5165 proteins were identified and quantified in sEVs and cell extracts. Then, statistical analysis was performed to identify dysregulated proteins. Moderated t-statistics expression ratios $\geq$1.5 (upregulated) or $\leq$0.67 (downregulated), and a p-value $\leq$0.05 were used for the identification of significantly dysregulated proteins. For the human HLE-B3 sEVs, seven proteins were identified as dysregulated, with four proteins showing

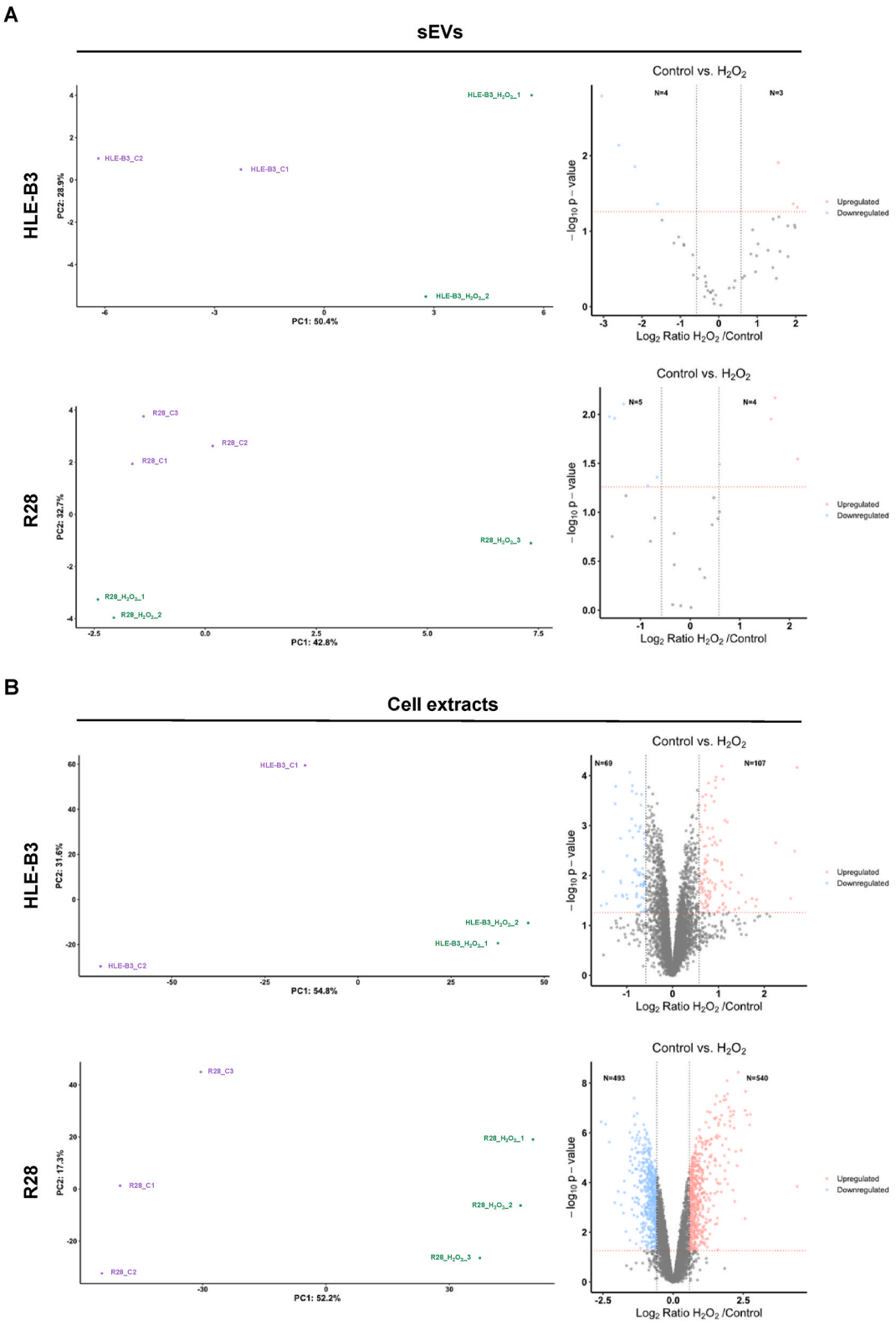

Fig. 2. Differential protein expression analysis of the 10-plex TMT quantitative proteomics experiments. Principal component analysis (PCA) showed the appropriate clustering of sEVs (A) and cell extracts replicates (B), but for the R28_H_2O_2_3 replicate. Volcano plots of both TMT experiments with sEVs (A) and cellular extracts (B) of rat R28 and human HLE-B3 cells represent dysregulated proteins in H_2O_2 stress induced cells with an expression ratio$\geq$ 1.5 and p-value $\leq$0.05. Proteins represented in blue undergone downregulation, whereas upregulated proteins are represented in red. Dashed red line represents p-value = 0.05, whereas a 1.5-fold expression difference is represented by two black dashed vertical lines. (For interpretation of the references to colour in this figure legend, the reader is referred to the Web version of this article.)

downregulation and three upregulation upon oxidative stress induction (Fig. 2A and Supplementary Table 3). Regarding the analysis of sEVs from R28 cells, five proteins showed downregulation and four of them showed upregulation upon H_2O_2 incubation (Fig. 2A and Supplementary Table 3). On the other hand, a total of 176 dysregulated proteins were identified in human HLE-B3 cell extracts, with 69 proteins downregulated and 107 proteins upregulated in HLE-B3 H_2O_2 cells (Fig. 2B and Supplementary Table 3). Moreover, the induction of the R28 cell line with H_2O_2 resulted in the dysregulation of a total of 1033 proteins, with 493 downregulated proteins and 540 upregulated proteins (Fig. 2B and Supplementary Table 3).

Thus, we subsequently performed a gene ontology analysis to investigate the enriched biological processes and cell component, where the identified and dysregulated proteins were involved (Fig. 3). Processes represented in the plots were the most significantly enriched ones (FDR< 0.05). Our analysis revealed that most of the proteins identified in HLE-B3 sEVs were related to immune response, while most of the proteins identified in R28 sEVs were associated with cell junctions and metabolic pathways. Importantly, in both cell sEVs samples, secretory vesicles and/or secretory granule proteins were amongst the top ten processes, indicating the correct enrichment of extracellular vesicles (Fig. 3). In cell extracts, proteins involved in the regulation of cell division, oxidation-reduction processes, metabolic pathways, and/or regulation of cellular localization in both cell lines upon oxidative stress induction were observed likely to compensate for the damage associated to oxidative stress (Fig. 3). As expected because of the induction of oxidative stress, String and Reactome analysis of identified proteins in cell extracts revealed that exposure to H_2O_2 in HLE-B3 and R28 cells led to alterations in the expression of proteins belonging to processes related to the regulation of oxidative stress with proteins having an antioxidant role in redox homeostasis (pathway significance: FDR< 0.05), contributing to the elimination of generated free radicals (Figs. 4 and 5, Supplementary Fig. 2, and Supplementary Fig. 3). Additionally, proteins related to DNA repair, lipid metabolism, mitosis regulation, and mitochondrial translation were also identified (FDR< 0.05) (Figs. 4 and 5, Supplementary Fig. 2, and Supplementary Fig. 3).

3.3. Validation of dysregulated proteins in cell extracts

Next, 21 proteins were selected for validation according to their expression ratio and the reagent availability for WB (Table 2). Thus, from the TMT experiment with sEVs, we selected for validation by WB with cell extracts 3 proteins out of the 7 and 9 dysregulated proteins observed in HLE-B3 and R28's sEVs, respectively: COL1A1 (upregulated in both H_2O_2 cell lines), ACTA2 (upregulated in H_2O_2 R28 sEVs), and DBF4B (upregulated in H_2O_2 HLE-B3 sEVs). Importantly, selected proteins were previously detected in sEVs of other diseases, highlighting the strength of the proteomics analysis performed. Since experimental validation with sEVs was challenging due to the low number of sEVs produced by the cells, cell extracts were used to perform validation assays either with proteins upregulated or downregulated by proteomics in sEVs and cell extracts. Additionally, as we obtained a higher number of dysregulated proteins from the TMT analyses with cell extracts (1033 and 176 for R28 and HLE-B3 cells, respectively), 9 proteins (4 upregulated and 5 downregulated), for each cell line, with the highest expression ratio and available antibodies were selected for validation (Table 2).

Then, total cell extracts from HLE-B3 and R28 cells were first analyzed by WB (Fig. 6). First, COL1A1 and DBF4B were found in an opposite dysregulated trend in HLE-B3 cell extracts than in their corresponding sEVs, whereas COL1A1 and ACTA2 were confirmed as upregulated in the cell extracts of R28 cells. On the other hand, the dysregulation observed by proteomics in the cell extracts was confirmed by WB in the specific cell line where the protein was detected as dysregulated. In H_2O_2 HLE-B3 extracts, GCOM1 and FAM213A proteins showed the highest increases, whereas the most pronounced decreases were assessed for RAD23B and SPARC proteins. Regarding H_2O_2 R28 extracts, noticeable increments were detected for DNAJC15 and MIPEP proteins and the most remarkable decreases were found for MAGI1 and AARS2 proteins.

3.4. Analysis of selected validated dysregulated proteins in aqueous humors

Additionally, as we used these cells upon oxidative stress induction as models of cataracts and glaucoma eye pathologies, we hypothesized whether these proteins could also be altered in human aqueous humors from cataracts or glaucoma patients in comparison to aqueous humor of individuals without any of these pathologies (ICL), either using pools or individual samples.

To address this question, we analyzed patients and ICL's aqueous humor samples by WB (Fig. 7). Importantly, despite the change from cell models to human samples, WB of pooled and individual aqueous humor samples confirmed, at least in part, the dysregulations observed by mass spectrometry in our cell models for cataracts and glaucoma. COL1A1, DBF4B, and SPARC exhibited trends similar to those observed by proteomics, but their changes did not reach statistical significance. Moreover, two different isoforms were observed for COL3A1, showing the upper band an opposite dysregulation to that determined by proteomics, although statistically significant, whereas the lower band showed a similar dysregulation as observed by proteomics in glaucoma without statistical significance. Furthermore, a similar dysregulation to that determined by proteomics and statistically significant differences were found for ACTA2, MAGI1, GCOM1, and RAD23B, indicating their potential as markers of these eye pathologies by their measurement in aqueous humors (Fig. 7). The differences observed in COL3A1 between validation in aqueous humors and proteomics results could be related to the use of total aqueous humor samples instead of sEVs isolated from aqueous humors. Besides, in addition to lens epithelial cells or ganglion cells, aqueous humor comprises proteins produced by different ocular cellular structures from the anterior and posterior segment. Likewise, the cell model, although useful, could not perfectly resemble the disease conditions in the eye and in aqueous humors.

3.5. Diagnostic ability of RAD23B protein levels in aqueous humor

Next, we assessed whether these proteins could serve as markers of glaucoma by ELISA. According to reagent availability, we focused on analyzing and quantifying the protein levels of RAD23B by commercially available ELISA with a higher number of samples using directly human aqueous humors from glaucoma patients (N = 24) in comparison to cataracts (N = 28) and ICL samples (N = 28) (Fig. 8). The mean concentration in pg/mL for RAD23B was 10853.97 in ICL individuals, 10886.51 in cataracts patients, and 10350.46 in glaucoma patients' samples. Importantly, a non-statistical significance for RAD23B concentration was detected between ICL and cataracts subjects, whereas, RAD23B showed ability to discriminate between glaucoma and ICL subjects as well as between glaucoma and cataracts patients. Moreover, RAD23B results were equivalent between controls and glaucoma (Fig. 8A), and between controls and cataracts combined in comparison to glaucoma (Supplementary Fig. 4). Noticeable, as we observed that the age of controls was lower than that of the pathological individuals, and indeed, there were statistical differences in the age of ICL (healthy) individuals in comparison with the pathological individuals (p value = 1×10^{-14} healthy vs cataracts, p value = 1.58×10^{-12} healthy vs glaucoma), but not between cataracts and glaucoma patients (p value = 0.2856 cataracts vs glaucoma), RAD23B ELISA results indicated that the changes in this marker were related to glaucoma pathology despite the age of the individuals analyzed. Thus, ELISA results demonstrate that the marker was associated to glaucoma and not to aging.

Next, the area under the curve (AUC), specificity, and sensitivity of this potential glaucoma aqueous humor biomarker were determined by

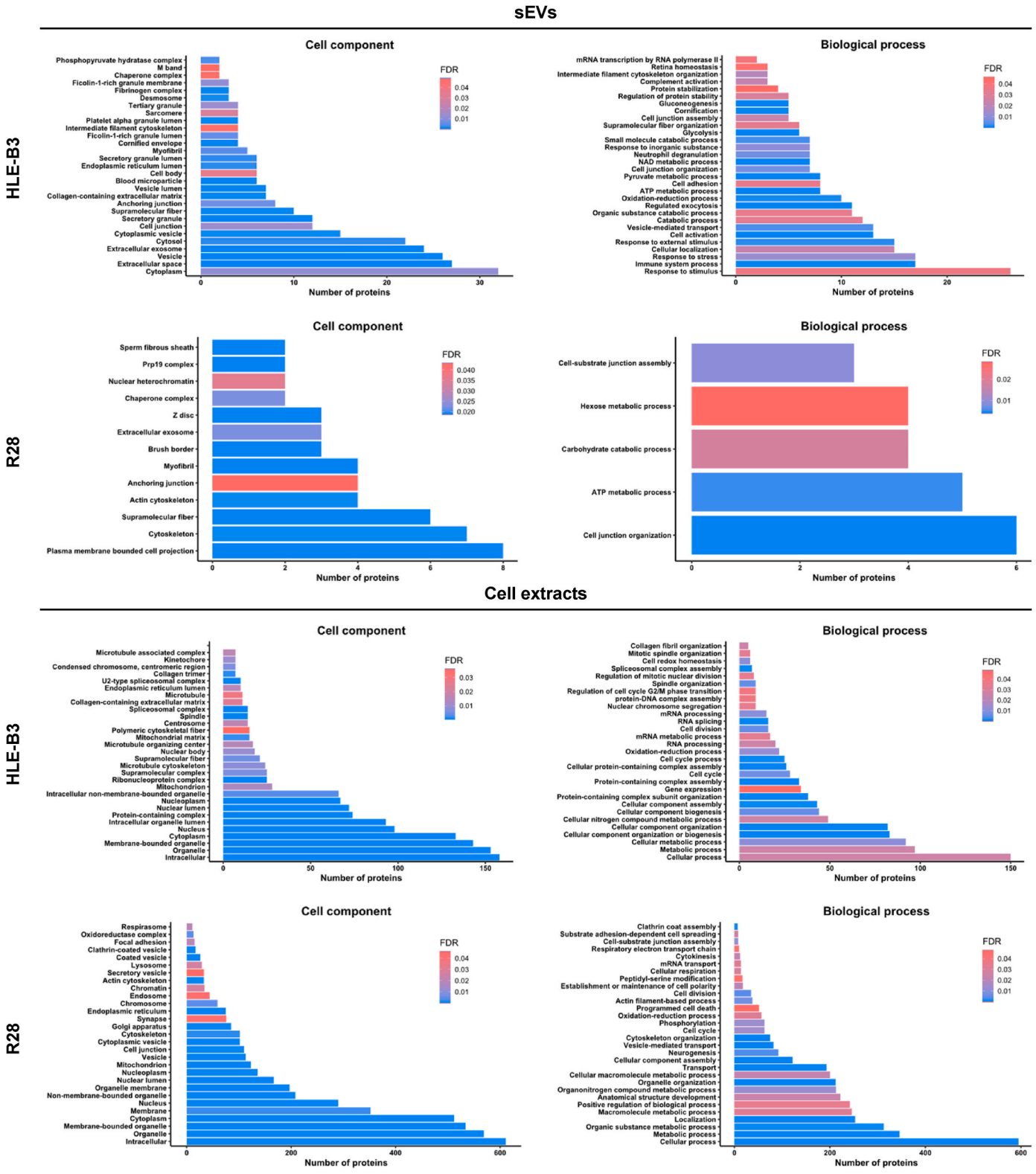

Fig. 3. Gene Ontology analysis of identified proteins. The identified proteins were functionally classified based on universal Gene Ontology (GO) annotation terms into two categories: cellular component and biological process. Bar length is proportional to the number of proteins associated with the GO annotation. Statistically significant biological processes (FDR <0.05) are shown in a red-blue scale. (For interpretation of the references to colour in this figure legend, the reader is referred to the Web version of this article.)

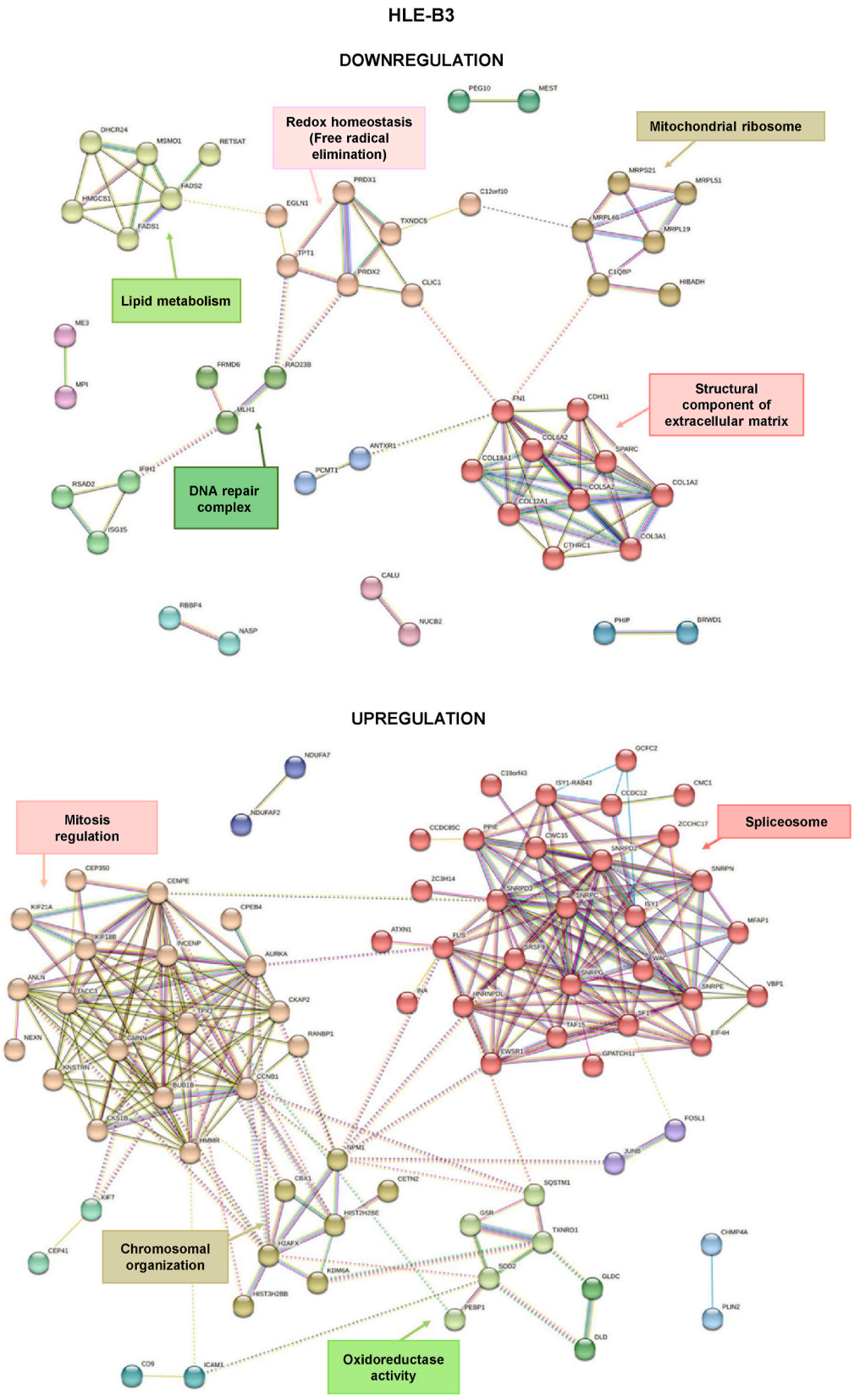

Fig. 4. Protein interactome map of dysregulated proteins identified in HLE-B3 cells exposed to H_2O_2. String analysis of differentially expressed downregulated and upregulated proteins in HLE-B3 cells exposed to H_2O_2 in comparison with control (untreated) cells (FDR <0.05). String analysis revealed nine clusters of interaction (five for downregulated proteins and four for upregulated proteins) among the identified dysregulated proteins. Only clusters with two or more interconnected proteins are displayed.

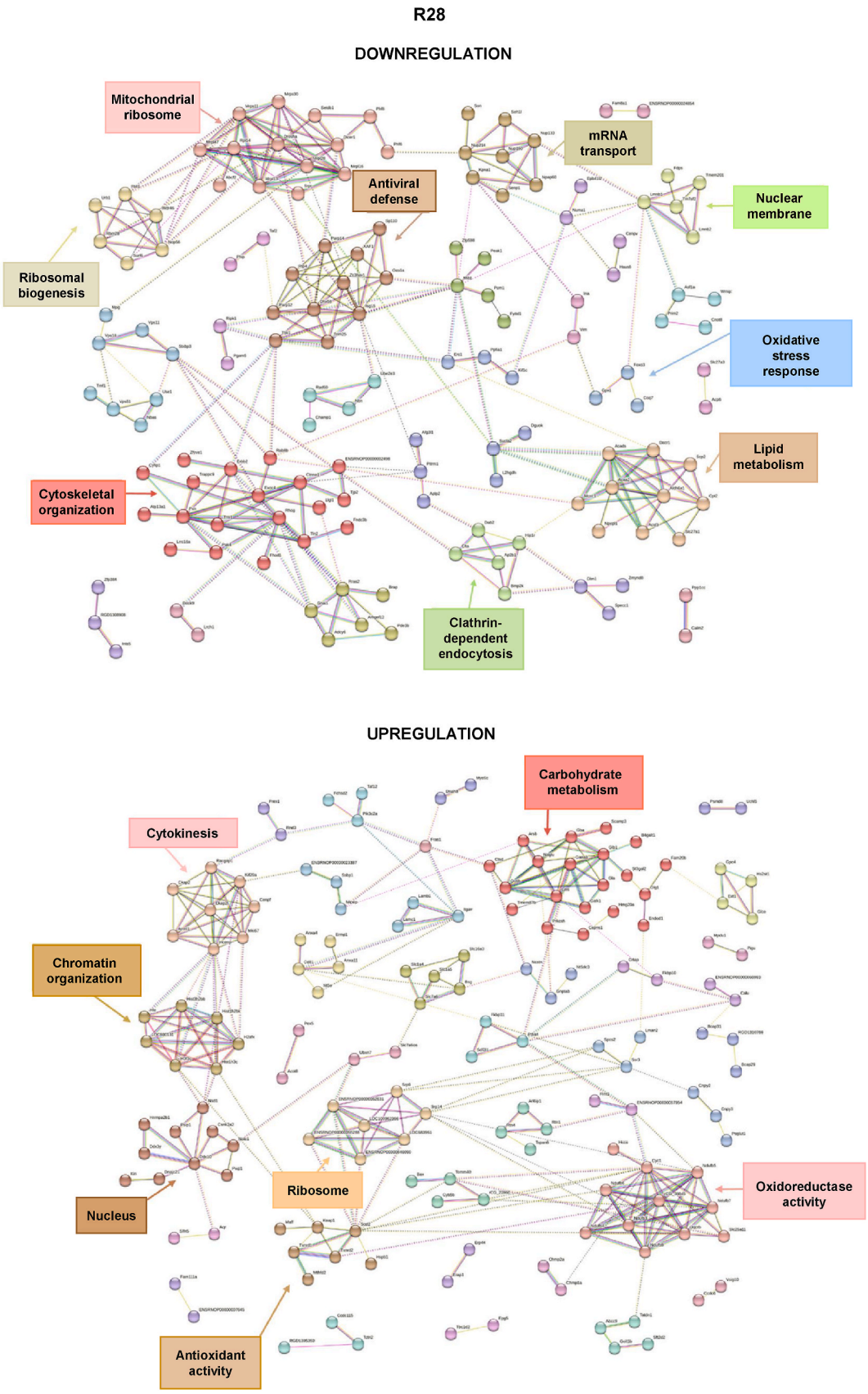

Fig. 5. Protein interactome map of dysregulated proteins identified in R28 cells exposed to H_2O_2. String analysis of downregulated and upregulated proteins differentially expressed in R28 cells exposed to H_2O_2 in comparison with control (untreated) cells (FDR <0.05). String analysis revealed sixteen clusters of interaction (nine for downregulated proteins and seven for upregulated proteins) among the identified dysregulated proteins. Only clusters with two or more interconnected proteins are displayed.

Table 2
Proteins selected for validation. 21 proteins were selected for validation among the total number of dysregulated proteins identified by TMT in HLE-B3 and R28 cells either in the cell extracts or in the sEVs.

		Protein name	Dysregulation	Fold Change	P value	Exocarta
TMT cell extracts	**HLE-B3**	ARP19	Upregulation	2.72	0.045	–
		TCEAL4	Upregulation	2.84	0.01	–
		GCOM1	Upregulation	3.51	0.04	–
		FAM213A	Upregulation	6.33	0.003	–
		RAD23B	Downregulation	0.34	0.04	–
		SPARC	Downregulation	0.35	0.008	–
		HMGCS1	Downregulation	0.42	0.0004	–
		COL3A1	Downregulation	0.42	0.0002	–
		CALU	Downregulation	0.47	0.025	–
	R28	DNAJC15	Upregulation	4.1	2.83E-07	–
		MIPEP	Upregulation	4.48	1.23E-07	–
		KIN17	Upregulation	4.51	5.10E-07	–
		SV2B	Upregulation	6.72	1.07E-07	–
		CDKN2A	Downregulation	0.34	3.04E-05	–
		CALM	Downregulation	0.34	0.02	–
		MAGI1	Downregulation	0.36	0.001	–
		ITPR1	Downregulation	0.36	9.07E-06	–
		AARS2	Downregulation	0.58	1.24E-05	–
TMT cell sEVs	**HLE-B3**	**DBF4B**	Upregulation	4.12	0.04	Mesenchymal stem cells
		COL1A1	Upregulation	2.96	0.05	Endothelial cells, melanoma cells, mesenchymal stem cells, prostate cancer cells and thymus
	R28	**ACTA2**	Upregulation	1.51	0.03	Colorectal cancer cells, keratinocytes, mesenchymal stem cells, platelets, prostate cancer cells and urine
		COL1A1	Upregulation	4.48	0.03	Endothelial cells, melanoma cells, mesenchymal stem cells, prostate cancer cells and thymus

means of ROC curves (Fig. 8A). The AUC for discriminating glaucoma patients from ICL or cataracts were 73.44 %, and 68.9 % for RAD23B, respectively, with potential to discriminate between cataracts and glaucoma patients with an AUC of 68.9 %, and a sensitivity and specificity of 66.67 % and 67.86 %, respectively. Additionally, as we have recently patented (P202430051) two glaucoma biomarkers in small extracellular vesicles isolated from aqueous humor samples, GAS6 and SPP1 [38], we finally investigated whether their combination with RAD23B would increase the diagnostic effectiveness of glaucoma patients from cataracts patients and/or from ICL individuals. Remarkably, RAD23B in combination with SPP1 and GAS6 increased the ability of the two-protein panel to discriminate glaucoma patients from ICL individuals or from cataracts patients, with AUCs of 83.50 % and 71.90 %, respectively, and specificities and sensitivities higher than 65 % and 79 %, respectively (Fig. 8B).

Collectively, these results highlight the predictive value of RAD23B for the discrimination of glaucoma patients from ICL individuals and cataracts patients. Our analysis also confirms the improvement of the predictive capacity of RAD23B in combination with the other two protein markers previously described, and thus, potentially allowing for an earlier identification of glaucoma patients during ocular surgery.

4. Discussion

This study aims to deepen the existing knowledge on the proteomics of cataracts and glaucoma, providing new insights into proteins whose expression is altered under oxidative stress, a key pathological event in both diseases. To simulate oxidative stress and mimic an experimental cataract and glaucomatous model to analyze potential proteomics dysregulation compared to untreated control cells, HLE-B3 and R28 cells, respectively, were treated with H_2O_2. Then, the protein profile of sEVs released by cells as well as protein content in cell extracts was evaluated by LC-MS/MS. The goal of the work consisted not only of identifying these altered proteins, but also analyzing their potential as diagnostic biomarkers. In this sense, we hypothesized that the cellular models subjected to ROS could mimic, at least in part, the observed behavior in cataracts and/or glaucoma patients. Consequently, we validated the dysregulated protein expression in aqueous humor from patients with these pathologies as compared to control subjects and analyzed their potential as diagnostic biomarkers.

After sEVs isolation, nanoparticle tracking analysis revealed a multimodal distribution with the presence of heterogeneous sEVs in size, exhibiting the predominant peaks a size compatible with sEVs. Moreover, a different size distribution of sEVs was detected after oxidative stress exposure in the ocular cells as compared with control cells. This could be a limitation of our study as it might be some bias towards the isolation of more heterogenous sEVs due to the stress oxidative conditions but not related to technical reproducibility since sEVs possessed a similar size distribution among different isolations. In this sense, previous reports have indicated changes in the sEVs morphology [39] and yield [40] in response to oxidative stress in cells. An increase in multivesicular bodies was promoted by low oxidative stress whereas higher ROS led to multivesicular bodies degradation by inducing autophagy [40]. Human retinal astrocytes treated with *tert*-butyl hydroperoxide, as oxidative stress inductor, released larger size and a smaller quantity of exosomes as compared to control cells [41]. Different EVs morphological characteristics and EVs budding profiles were identified in human neuroblastoma wild-type SH-SY5Y cells in basal conditions and after oxidative stress induction with a significant shift toward wider size distribution and an increase in the average diameter of EVs after treatment [39]. In contrast, a reduction of EVs size was detected in SOD1-G93A SH-SY5Y cells after H_2O_2 treatment [39], indicating that oxidative stress effect on EVs's size is cell-type specific. In this sense, a different behavior regarding sEVs size was detected for HLE-B3 and R28

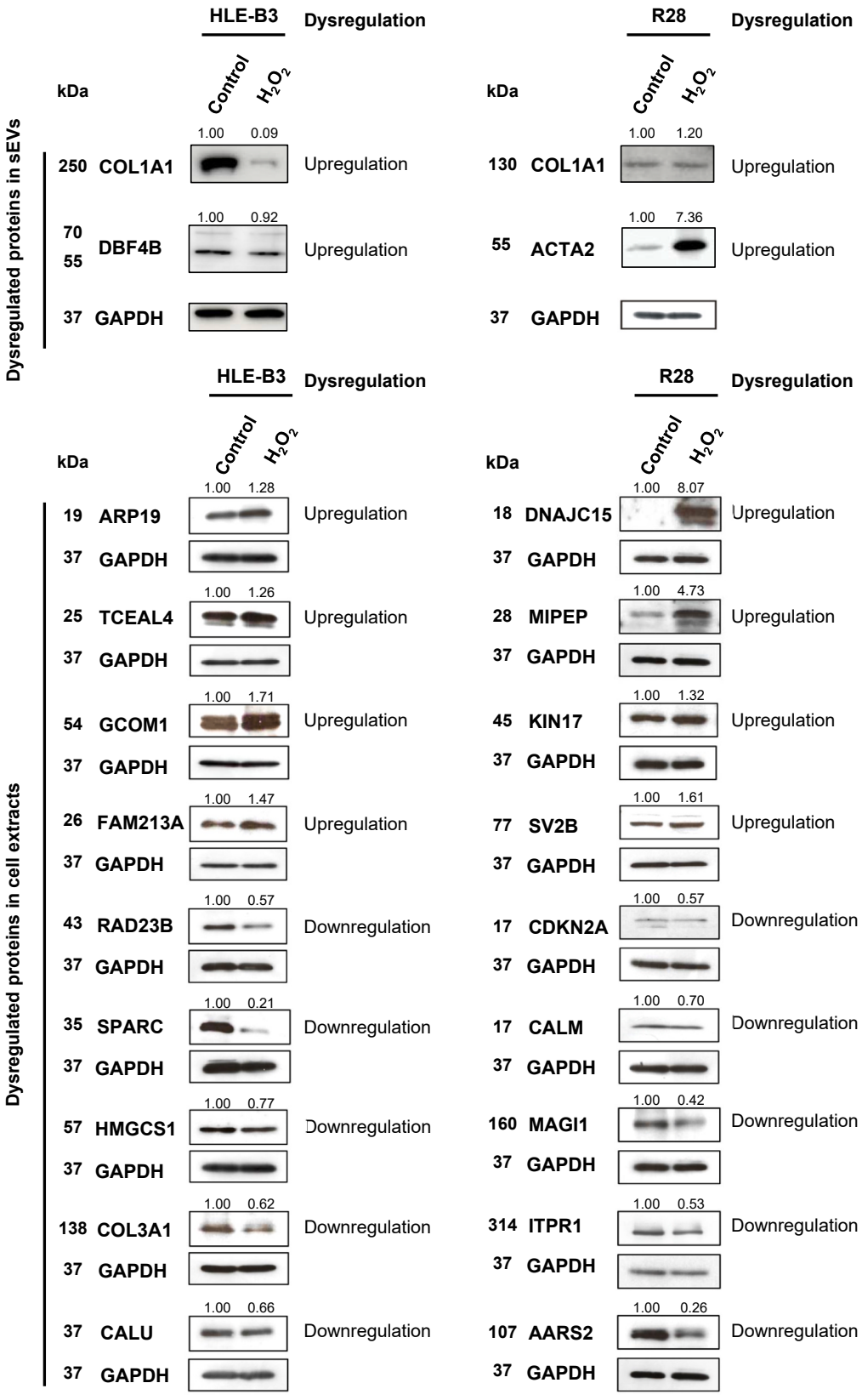

Fig. 6. Validation of proteomics results by WB analysis using cell protein extracts from HLE-B3 and R28 cells. The dysregulation of indicated dysregulated proteins from the sEVs and cell extracts TMT experiments was confirmed by WB using cell protein extracts from control and H_2O_2 induced HLE-B3 and R28 ocular cell lines. For each protein, the type of dysregulation detected in the TMT quantitative proteomics analysis is indicated. Protein band intensities were normalized according to the GAPDH protein band.

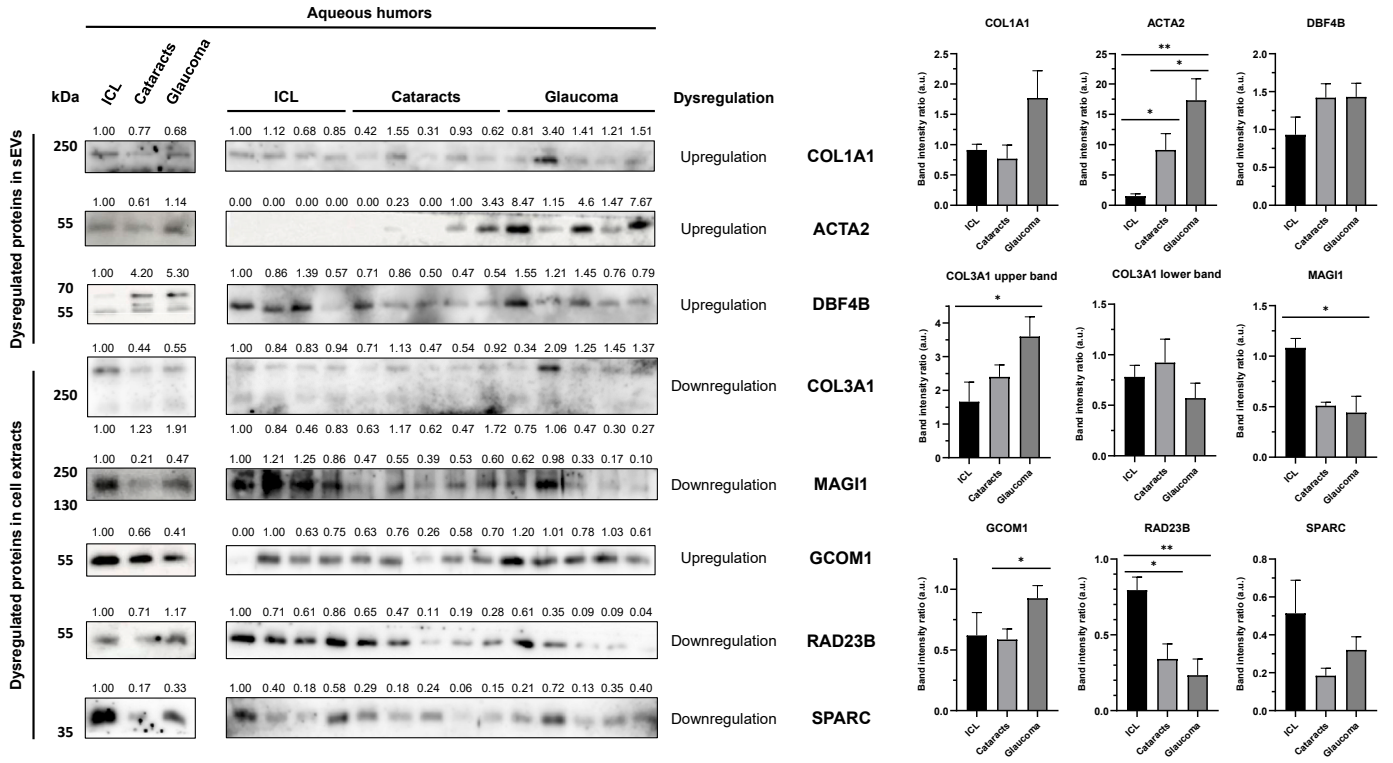

Fig. 7. Analysis in aqueous humor samples of selected dysregulated proteins by WB. Pooled aqueous humors from ICL (n = 4 individuals) individuals, and cataracts (n = 5) and glaucoma (n = 4) patients, and individual aqueous humor samples from ICL (N = 4), and cataracts (N = 5), and glaucoma (N = 5) patients were used to evaluate the dysregulation of indicated proteins from the sEVs and cell extracts TMT for HLE-B3 and R28 cell lines. For each protein, the type of dysregulation detected in the TMT quantitative proteomics analysis is indicated. Coomassie blue staining and Ponceau red staining were used to compare the protein content and the protein band intensities were normalized according to the GAPDH protein band. The statistical analysis performed is shown in histograms.

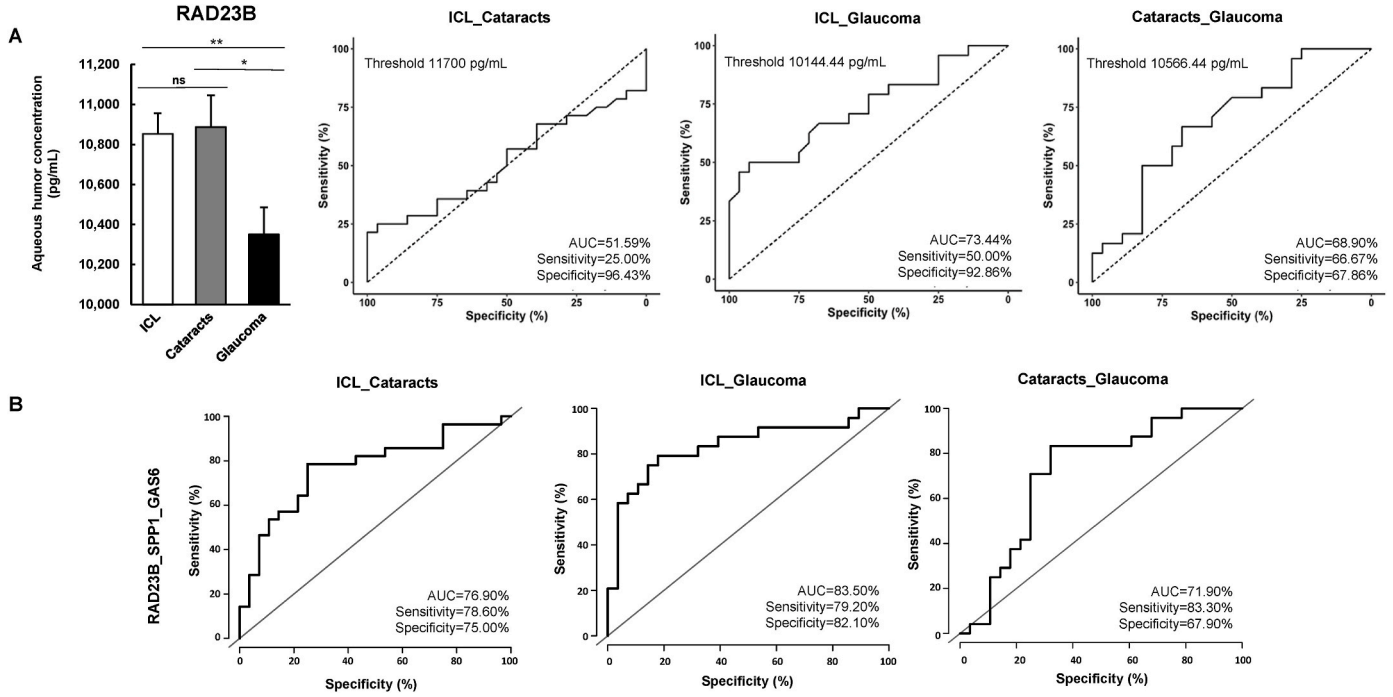

Fig. 8. Analysis in aqueous humor samples of selected dysregulated proteins by ELISA. A) ELISA and ROC curves analyses of RAD23B levels in aqueous humor samples from ICL (N = 28) individuals, and cataracts (N = 28) and glaucoma (N = 24) patients showed significantly lower RAD23B protein levels in glaucoma aqueous humor samples than in ICL and cataracts samples, with a diagnostic ability higher than 70 % to discriminate glaucoma patients from ICL individuals and of 68.90 % to discriminate glaucoma patients from cataracts patients. B) The combination of RAD23B with previously identified SPP1 and GAS6 glaucoma biomarkers increased RAD23B diagnostic ability of glaucoma up to 83 %, with a sensitivity higher than 79 %, and specificity higher than 65 %.

cells exposed to oxidative stress.

Additionally, changes induced by oxidative stress, not only in morphology and yield, but also in sEVs content have been reported in ocular cells [42]. Our in-depth proteomics study on lens epithelial and retinal ganglionar sEVs resulted in the identification of 7 and 9 dysregulated proteins, respectively, with an expression ratio≥1.5. WB analysis partly confirmed the proteomics data, whereas the different trend detected in COL1A1 and DBF4B in HLE-B3 cells would be associated to the fact that the validation was performed using cell extracts instead of sEVs. In the aqueous humors, COL1A1, DBF4B, and ACTA2 exhibited trends similar to those found by proteomics, but only the changes in ACTA2 protein expression were statistically significant. Among the dysregulated proteins present in sEVs from HLE-B3 cells, IGKC was detected, the presence of this protein has been previously determined in the aqueous humor from cataract patients [43]. Interestingly, in sEVs from R28 cells exposed to oxidative stress, downregulation of ENO1, ALDOART2, and PRDX1 proteins were found. ENO1 is a very abundant protein present in different regions of the retina [44] and previous proteomics analysis revealed decrease expression of this protein in aqueous humor from patients with glaucoma and a significant correlation with clinical parameters [45]. Similarly, downregulation of ALDOART2 and the antioxidative protein PRDX1 were assessed in aqueous humor from glaucoma patients [46]. Likewise, FN1 and C4A proteins detected as dysregulated in sEVs from R28 cells exposed to oxidative stress, were also determined in aqueous humors from patients with glaucoma showing a significant correlation with visual field parameters [47]. The detection of these protein changes in the glaucomatous aqueous humor supports the importance of analyzing ROS induced protein changes in retinal ganglion cells and corroborates the evidence that oxidative damage accompanies glaucoma progression.

On the other hand, our in-depth proteomics study on lens epithelial cell extracts and retinal ganglionar cells, allow us identifying 69 and 493 downregulated proteins and 107 and 540 upregulated proteins, respectively, with an expression ratio≥1.5. Upregulation of proteins was more prevalent in both cell lines than downregulation in the presence of ROS. Moreover, a higher number of dysregulated proteins were detected in R28 cells exposed to oxidative stress than in HLE-B3 cells, which is concordant with the fact that retinal ganglion cells have higher energy requirements and are particularly susceptible to oxidative stress damage and mitochondrial impairment [48]. Validation of altered proteins by WB using cell extracts and aqueous humors partially confirmed mass spectrometry-based proteomics findings, in spite of not reaching statistical significance in all the proteins evaluated in the patient's aqueous humor.

The determination of functional relationships between identified dysregulated proteins using String and Reactome analysis helps comprehend how protein interactions were altered upon oxidative stress induction, shedding light on the significance of the dysregulated proteins in particular biological process. In both cell lines, clusters of oxidative stress response were identified in both downregulated and upregulated protein analyses. In HLE-B3 cells, downregulation of peroxiredoxin 1 and 2 (PRDX1 and PRDX2) by oxidative stress inductions was detected. In previous studies using CD5A lens epithelial cells, the exposure to oxidative stress caused a decrease in the non-oxidized form (active form) of the enzyme PRDX1, reducing the antioxidant defense provided by PRDX1 [49]. Regarding the induction of proteins by oxidative stress to protect the cell from oxidative damage, we could observe the enzyme SOD2 among the proteins upregulated in the oxidoreductase activity cluster. Previous studies have shown an increase in the expression of this enzyme modulated by the antioxidant factor NRF2 after exposure to photooxidation in HLE-B3 cells [50], and the NRF2/KEAP1 pathway display a central role regulating defense mechanisms against oxidative stress. In R28 cells, three different clusters associated with oxidative stress (oxidative stress response, antioxidant activity, and oxidoreductase activity) were determined. These clusters comprised 21 proteins including FOXO3, KEAP1, SOD2, HSPB1, and SLC25A11. Additionally, in both cell lines there were other relevant clusters related to nuclear functions, including some essential ones involved in DNA repair, and lipid metabolism. Changes in lipid synthesis could be due to oxidative stress metabolic response in cataracts and glaucoma and may play a potential contribution in the pathophysiology of these diseases. In this sense, it has been demonstrated that aqueous humor lipid composition of glaucoma patients differs from healthy individuals [51].

It is also noteworthy that some of the identified proteins in the clusters of R28 cells were directly related to clusters established in proteomics studies using different experimental animal models of glaucoma. In this sense, the upregulation of transporter clusters has been observed in proteomics studies based on retinas from experimental glaucoma animal models induced by elevated intraocular pressure [52], optic nerve crush [53], as well as in retinas from patients with glaucoma [54]. In our study an upregulated cluster of proteins consisting of a family of transporters (SLCLA4, SLC7A6, SLCLA5, and SLC16A3) was observed.

While information about the direct relationship of many of the proteins identified in cellular extracts with cataracts and glaucoma is scarce, there are data available for some of them. RAD23B (with a decreased cellular expression observed by mass spectrometry and confirmed by WB in our study), plays essential roles in nuclear excision repair, damage recognition, and proteasome regulation [55]. It has been suggested that the increase of this protein is related to the protective effect of ginsenosides against apoptosis induced by H_2O_2 in human lens epithelial cells [56]. A decreased in SPARC protein levels was also observed by proteomics and confirmed by WB. Previous studies have demonstrated the key role that SPARC plays in maintaining the structural integrity and transparency of the lens [57,58], suggesting that changes in its expression could contribute to cataractogenesis. SPARC was located within the cluster involved in the extracellular matrix structure together with COL3A1, which was also downregulated in H_2O_2 HLE-B3 cell extracts. In human trabecular cells, SPARC is a component of the signaling network that regulates the expression of α1 chains of collagens I and III and a similar function could be exercised in lens epithelial cells [59].

Regarding association with glaucomatous pathology, CALM2, CDKN2A, and ITPR1 were observed among the downregulated proteins associated to R28 cells by oxidative stress. Previous studies analyzing protein-protein interactions in a mutational region of chromosome 2 in families affected by primary open-angle glaucoma have considered the calmodulin 2 gene as related to changes in the trabecular meshwork and progressive loss of retinal ganglion cells in glaucoma patients [60]. Single-nucleotide polymorphisms in CDKN2B-AS locus are associated with human glaucoma [61]. CDKN2A expression was altered in experimental animal models of glaucoma and CDKN2A deficiency ameliorated retinal ganglion cell death [62,63], indicating that this protein is a vital regulator of retinal ganglion cell death in pathologic conditions. ITPR1 has been previously described as a protein specifically altered in aqueous humor from primary open glaucoma patients as compared with cataract and other type of glaucoma samples [64].

Finally, one of the main goals of the study consisted of validating the dysregulated proteins as biomarkers of glaucoma in aqueous humors. We focused on the analysis of RAD23B, amongst the highest dysregulated proteins, by ELISA to determine its potential as glaucoma biomarker. RAD23B protein levels were able to discriminate control individuals and cataracts patients from glaucoma patients with significant diagnostic ability by ELISA, demonstrating its role as a potential glaucoma biomarker in aqueous humors. AUC values to distinguish glaucoma patients from control or cataracts patients were about 70 % (73.44 % for ICL *vs* glaucoma and 68.9 % for cataracts *vs* glaucoma). A similar discriminating accuracy has been established for previously described glaucoma's biomarkers. Thus, aqueous humor metabolites such as 3′-sialyllactose or 2-methylbenzoic acid showed AUC values of 73 and 75 % respectively, for primary open angle glaucoma screening

[65]. ROC analysis also revealed AUC values around 70 % for plasma lactoferrin levels [66] and redox index (the log reduced glutathione/oxidized glutathione) [67] as potential diagnostic glaucoma biomarkers. On the other hand, AUC values above 70 % were determined for aqueous humor clusterin as biomarker of pseudoexfoliative glaucoma (AUC = 79 %) [68]. Likewise, AUC values between 70 and 80 % were calculated for VTN, TTR, SERPINA1, and FCN3 proteins when glaucoma patients and control subjects were compared, and higher than 80 % for TF, C3, and APOA4, although the number of participants in the study was relatively small (n = 53) [69].

Additionally, in our study, the inclusion of two aqueous humors proteins recently patented by the group as biomarkers of glaucoma (GAS6 and SPP1) [38] increased RAD23B specificity and sensitivity percentages, improving the diagnostic efficiency of glaucoma patients (AUC = 83.50 % for ICL vs glaucoma; AUC = 71.90 % for cataracts vs glaucoma). The design of diagnostic tests with multiple biomarkers can improve the diagnostic accuracy. In this way, the use of a biomarker panel consisted of five autoantibodies identified by serological proteome analysis yielded an AUC of 87 % [70]. Higher AUC values (90 %) were found using machine learning algorithms based on 28 aqueous humor immune mediators [71]. However, the translation of a diagnostic test with multiple biomarkers to clinical routine is challenging since the panel of identified biomarkers should be compact enough to be developed in a point-of-care device but robust enough to ensure specificity and sensitivity.

Finally, one limitation of the study is the significant difference of the age between ICL subjects (controls) and cataracts and glaucoma patients because of the challenge in obtaining ICL elderly samples. The ICL group comprised individuals with a transparent lens undergoing refractive surgery. Refractive surgery in patients in their late adulthood (>60 years) is not so frequent, since patients over 60 years of age generally have worse outcomes in both myopic and hyperopic treatments [72]. Moreover, subjects in their late-adulthood are also more likely to have early stages of cataracts, and it would preclude its inclusion as controls. Moreover, although we cannot discard completely that some results using human aqueous humor samples could be related to aging, the significant results of ACTA2, MAGI1, and GCOM1 by WB, and RAD23B by WB and ELISA pointed out that the main findings of the study were associated with glaucoma and cataracts and not to aging.

5. Conclusion

Protein profile of sEVs released by lens epithelial cells and retinal ganglion cells exposed to ROS, as experimental models of cataract and glaucomatous, as well as protein content in cell extracts was determined by LC-MS/MS. Our findings revealed the potential of cellular eye models subjected to ROS to mimic cataracts and/or glaucoma pathologies associated to oxidative stress for the *in vivo* elucidation of potential glaucoma biomarkers. Additionally, our results could offer insights into the pathophysiology of glaucoma and cataracts, paving the way for the future evaluation of unknown molecular pathological mechanisms and the identification of alternative potential biomarkers to enhance diagnosis and treatment. Finally, as one of the most relevant goals of the study, we have gone here through the analyses by proteomics of ocular cell models of oxidative stress to the identification and validation of RAD23B as a downregulated protein in the aqueous humor of glaucoma patients with potential diagnostic ability of the disease in comparison with cataracts patients or control individuals used in the study as controls.

Funding

This study was supported with the financial support of the PR44/21–29922 grant from Santander-Complutense and PI23/00607 grant from the AES-ISCIII program, co-financed with FEDER funds to A.G-A. R. B. wants also to acknowledge PI20CIII/00019 and PI23CIII/00027 grants from the AES-ISCIII program cofounded by FEDER funds. The PFIS predoctoral contract to R.R-G. was supported by the AES-ISCIII AESIRRHH 2021–2022 call (contract Reference FI22CIII/00016).

Data availability

The mass spectrometry proteomics data have been deposited at the ProteomeXchange Consortium via the PRIDE partner repository with the dataset identifier PXD054459. The R code and R packages used in the manuscript are depicted in the material and methods section.

CRediT authorship contribution statement

Raquel Rejas-González: Writing – review & editing, Writing – original draft, Visualization, Investigation. **Ana Montero-Calle:** Writing – review & editing, Writing – original draft, Visualization, Investigation, Conceptualization. **Natalia Pastora Salvador:** Writing – review & editing, Investigation. **María José Crespo Carballés:** Writing – review & editing, Investigation. **Emma Ausín-González:** Writing – review & editing, Investigation. **Juan Sánchez-Naves:** Writing – review & editing, Investigation. **Sara Pardo Calderón:** Writing – review & editing, Investigation. **Rodrigo Barderas:** Writing – review & editing, Writing – original draft, Visualization, Funding acquisition, Conceptualization. **Ana Guzman-Aranguez:** Writing – review & editing, Writing – original draft, Visualization, Investigation, Funding acquisition, Conceptualization.

Declaration of competing interest

The authors declare that they have no known competing financial interests or personal relationships that could have appeared to influence the work reported in this paper.

Acknowledgments

The authors would like to acknowledge the instrumental and the excellent technical support of the Electronic Microscopy Unit of the Instituto de Salud Carlos III.

Appendix A. Supplementary data

Supplementary data to this article can be found online at https://doi.org/10.1016/j.redox.2024.103368.

References

[1] Y.C. Liu, M. Wilkins, T. Kim, B. Malyugin, J.S. Mehta, Cataracts, Lancet 390 (10094) (2017) 600–612, https://doi.org/10.1016/S0140-6736(17)30544-5.
[2] Y.C. Tham, X. Li, T.Y. Wong, H.A. Quigley, T. Aung, C.Y. Cheng, Global prevalence of glaucoma and projections of glaucoma burden through 2040: a systematic review and meta-analysis, Ophthalmology 121 (11) (2014) 2081–2090, https://doi.org/10.1016/j.ophtha.2014.05.013.
[3] D. Goodman, S. Ness, The role of oxidative stress in the aging eye, Life 13 (3) (2023), https://doi.org/10.3390/life13030837.
[4] M.A. Babizhayev, Y.E. Yegorov, Reactive oxygen species and the aging eye: specific role of metabolically active mitochondria in maintaining lens function and in the initiation of the oxidation-induced maturity onset cataract–A novel platform of mitochondria-targeted antioxidants with broad therapeutic potential for redox regulation and detoxification of oxidants in eye diseases, Am. J. Therapeut. 23 (1) (2016) e98–e117, https://doi.org/10.1097/MJT.0b013e3181ea31ff.
[5] O. Erol Tinaztepe, M. Ay, E. Eser, Nuclear and mitochondrial DNA of age-related cataract patients are susceptible to oxidative damage, Curr. Eye Res. 42 (4) (2017) 583–588, https://doi.org/10.1080/02713683.2016.1200100.
[6] X. Jin, H. Jin, Y. Shi, Y. Guo, H. Zhang, Pyroptosis, a novel mechanism implicated in cataracts, Mol. Med. Rep. 18 (2) (2018) 2277–2285, https://doi.org/10.3892/mmr.2018.9188.
[7] A. Spector, W.H. Garner, Hydrogen-peroxide and human cataract, Exp. Eye Res. 33 (6) (1981) 673–681, https://doi.org/10.1016/S0014-4835(81)80107-8.
[8] A. Spector, G.M. Wang, R.R. Wang, W.H. Garner, H. Moll, The prevention of cataract caused by oxidative stress in cultured rat lenses. I. H2O2 and photochemically induced cataract, Curr. Eye Res. 12 (2) (1993) 163–179, https://doi.org/10.3109/02713689308999484.

[9] F. Buonfiglio, E.W. Bohm, N. Pfeiffer, A. Gericke, Oxidative stress: a suitable therapeutic target for optic nerve diseases? Antioxidants 12 (7) (2023) https://doi.org/10.3390/antiox12071465.

[10] C. Benoist d'Azy, B. Pereira, F. Chiambaretta, F. Dutheil, Oxidative and anti-oxidative stress markers in chronic glaucoma: a systematic review and meta-analysis, PLoS One 11 (12) (2016) e0166915, https://doi.org/10.1371/journal.pone.0166915.

[11] B. Tang, S. Li, W. Cao, X. Sun, The association of oxidative stress status with open-angle glaucoma and exfoliation glaucoma: a systematic review and meta-analysis, J. Ophthalmol. 2019 (2019) 1803619, https://doi.org/10.1155/2019/1803619.

[12] M. Nita, A. Grzybowski, The role of the reactive oxygen species and oxidative stress in the pathomechanism of the age-related ocular diseases and other pathologies of the anterior and posterior eye segments in adults, Oxid. Med. Cell. Longev. 2016 (2016) 3164734, https://doi.org/10.1155/2016/3164734.

[13] S.C. Sacca, A. Izzotti, P. Rossi, C. Traverso, Glaucomatous outflow pathway and oxidative stress, Exp. Eye Res. 84 (3) (2007) 389–399, https://doi.org/10.1016/j.exer.2006.10.008.

[14] W.K. Ju, K.Y. Kim, J.D. Lindsey, M. Angert, K.X. Duong-Polk, R.T. Scott, J.J. Kim, I. Kukhmazov, M.H. Ellisman, G.A. Perkins, R.N. Weinreb, Intraocular pressure elevation induces mitochondrial fission and triggers OPA1 release in glaucomatous optic nerve, Invest. Ophthalmol. Vis. Sci. 49 (11) (2008) 4903–4911, https://doi.org/10.1167/iovs.07-1661.

[15] G. Tezel, Oxidative stress in glaucomatous neurodegeneration: mechanisms and consequences, Prog. Retin. Eye Res. 25 (5) (2006) 490–513, https://doi.org/10.1016/j.preteyeres.2006.07.003.

[16] G. Tezel, X. Yang, J. Cai, Proteomic identification of oxidatively modified retinal proteins in a chronic pressure-induced rat model of glaucoma, Invest. Ophthalmol. Vis. Sci. 46 (9) (2005) 3177–3187, https://doi.org/10.1167/iovs.05-0208.

[17] K.R. Martin, H. Levkovitch-Verbin, D. Valenta, L. Baumrind, M.E. Pease, H. A. Quigley, Retinal glutamate transporter changes in experimental glaucoma and after optic nerve transection in the rat, Invest. Ophthalmol. Vis. Sci. 43 (7) (2002) 2236–2243.

[18] G. Tezel, Molecular regulation of neuroinflammation in glaucoma: current knowledge and the ongoing search for new treatment targets, Prog. Retin. Eye Res. 87 (2022) 100998, https://doi.org/10.1016/j.preteyeres.2021.100998.

[19] S. Missiroli, I. Genovese, M. Perrone, B. Vezzani, V.A.M. Vitto, C. Giorgi, The role of mitochondria in inflammation: from cancer to neurodegenerative disorders, J. Clin. Med. 9 (3) (2020), https://doi.org/10.3390/jcm9030740.

[20] H. Chen, Y. Deng, X. Gan, Y. Li, W. Huang, L. Lu, L. Wei, L. Su, J. Luo, B. Zou, Y. Hong, Y. Cao, Y. Liu, W. Chi, NLRP12 collaborates with NLRP3 and NLRC4 to promote pyroptosis inducing ganglion cell death of acute glaucoma, Mol. Neurodegener. 15 (1) (2020) 26, https://doi.org/10.1186/s13024-020-00372-w.

[21] E. Bazzan, M. Tine, A. Casara, D. Biondini, U. Semenzato, E. Cocconcelli, E. Balestro, M. Damin, C.M. Radu, G. Turato, S. Baraldo, P. Simioni, P. Spagnolo, M. Saetta, M.G. Cosio, Critical review of the evolution of extracellular vesicles' knowledge: from 1946 to today, Int. J. Mol. Sci. 22 (12) (2021), https://doi.org/10.3390/ijms22126417.

[22] A.E. Grigor'eva, S.N. Tamkovich, A.V. Eremina, A.E. Tupikin, M.R. Kabilov, V. V. Chernykh, V.V. Vlassov, P.P. Laktionov, E.I. Ryabchikova, [Characteristics of exosomes andmicroparticles discovered in human tears], Biomed. Khim. 62 (1) (2016) 99–106, https://doi.org/10.18097/PBMC20166201099.

[23] W.M. Dismuke, P. Challa, I. Navarro, W.D. Stamer, Y. Liu, Human aqueous humor exosomes, Exp. Eye Res. 132 (2015) 73–77, https://doi.org/10.1016/j.exer.2015.01.019.

[24] M. Ragusa, C. Barbagallo, L. Statello, R. Caltabiano, A. Russo, L. Puzzo, T. Avitabile, A. Longo, M.D. Toro, D. Barbagallo, H. Valadi, C. Di Pietro, M. Purrello, M. Reibaldi, miRNA profiling in vitreous humor, vitreal exosomes and serum from uveal melanoma patients: pathological and diagnostic implications, Cancer Biol. Ther. 16 (9) (2015) 1387–1396, https://doi.org/10.1080/15384047.2015.1046021.

[25] S. Atienzar-Aroca, M. Flores-Bellver, G. Serrano-Heras, N. Martinez-Gil, J. M. Barcia, S. Aparicio, D. Perez-Cremades, J.M. Garcia-Verdugo, M. Diaz-Llopis, F. J. Romero, J. Sancho-Pelluz, Oxidative stress in retinal pigment epithelium cells increases exosome secretion and promotes angiogenesis in endothelial cells, J. Cell Mol. Med. 20 (8) (2016) 1457–1466, https://doi.org/10.1111/jcmm.12834.

[26] L. Biasutto, A. Chiechi, R. Couch, L.A. Liotta, V. Espina, Retinal pigment epithelium (RPE) exosomes contain signaling phosphoproteins affected by oxidative stress, Exp. Cell Res. 319 (13) (2013) 2113–2123, https://doi.org/10.1016/j.yexcr.2013.05.005.

[27] J. Martinez-Garcia, B. Fernandez, A. Alvarez-Barrios, L. Alvarez, H. Gonzalez-Iglesias, R. Pereiro, Determination of endogenous trace elements in extracellular vesicles secreted by an in vitro model of human retinal pigment epithelium under oxidative stress conditions using ICP-MS, Talanta 263 (2023) 124693, https://doi.org/10.1016/j.talanta.2023.124693.

[28] J. Luo, P. Li, L. Kang, M. Ji, T. Zhou, B. Qin, J. Zhang, H. Guan, Exosomal microRNA-222-3p increases UVB sensitivity of lens epithelium cells by suppressing MGMT, Int. Ophthalmol. 43 (5) (2023) 1611–1628, https://doi.org/10.1007/s10792-022-02560-7.

[29] R. Wang, J. Li, X. Zhang, X. Zhang, X. Zhang, Y. Zhu, C. Chen, Z. Liu, X. Wu, D. Wang, M. Dongye, J. Wang, H. Lin, Extracellular vesicles promote epithelial-to-mesenchymal transition of lens epithelial cells under oxidative stress, Exp. Cell Res. 398 (1) (2021) 112362, https://doi.org/10.1016/j.yexcr.2020.112362.

[30] A. Montero-Calle, I. Aranguren-Abeigon, M. Garranzo-Asensio, C. Poves, M. J. Fernández-Aceñero, J. Martínez-Useros, R. Sanz, J. Dziaková, J. Rodriguez-Cobos, G. Solís-Fernández, E. Povedano, M. Gamella, R.M. Torrente-Rodríguez, M. Alonso-Navarro, V. de los Ríos, J.I. Casal, G. Domínguez, A. Guzman-Aranguez, A. Peláez-García, J.M. Pingarrón, S. Campuzano, R. Barderas, Multiplexed biosensing diagnostic platforms detecting autoantibodies to tumor-associated antigens from exosomes released by CRC cells and tissue samples showed high diagnostic ability for colorectal cancer, Engineering 7 (10) (2021) 1393–1412, https://doi.org/10.1016/j.eng.2021.04.026.

[31] A. Montero-Calle, A. Lopez-Janeiro, M.L. Mendes, D. Perez-Hernandez, I. Echevarria, I. Ruz-Caracuel, V. Heredia-Soto, M. Mendiola, D. Hardisson, P. Argueso, A. Pelaez-Garcia, A. Guzman-Aranguez, R. Barderas, In-depth quantitative proteomics analysis revealed C1GALT1 depletion in ECC-1 cells mimics an aggressive endometrial cancer phenotype observed in cancer patients with low C1GALT1 expression, Cell. Oncol. 46 (3) (2023) 697–715, https://doi.org/10.1007/s13402-023-00778-w.

[32] A. Montero-Calle, R. Coronel, M. Garranzo-Asensio, G. Solis-Fernandez, A. Rabano, V. de Los Rios, M.J. Fernandez-Acenero, M.L. Mendes, J. Martinez-Useros, D. Megias, M.T. Moreno-Casbas, A. Pelaez-Garcia, I. Liste, R. Barderas, Proteomics analysis of prefrontal cortex of Alzheimer's disease patients revealed dysregulated proteins in the disease and novel proteins associated with amyloid-beta pathology, Cell. Mol. Life Sci. 80 (6) (2023) 141, https://doi.org/10.1007/s00018-023-04791-y.

[33] A. Montero-Calle, M. Garranzo-Asensio, R. Rejas-Gonzalez, J. Feliu, M. Mendiola, A. Pelaez-Garcia, R. Barderas, Benefits of FAIMS to improve the proteome coverage of deteriorated and/or cross-linked TMT 10-plex FFPE tissue and plasma-derived exosomes samples, Proteomes 11 (4) (2023), https://doi.org/10.3390/proteomes11040035.

[34] A. Montero-Calle, S. Jimenez de Ocana, R. Benavente-Naranjo, R. Rejas-Gonzalez, R.A. Bartolome, J. Martinez-Useros, R. Sanz, J. Dziakova, M.J. Fernandez-Acenero, M. Mendiola, J.I. Casal, A. Pelaez-Garcia, R. Barderas, Functional proteomics characterization of the role of SPRYD7 in colorectal cancer progression and metastasis, Cells 12 (21) (2023), https://doi.org/10.3390/cells12212548.

[35] A. Montero-Calle, M. Gomez de Cedron, A. Quijada-Freire, G. Solis-Fernandez, V. Lopez-Alonso, I. Espinosa-Salinas, A. Pelaez-Garcia, M.J. Fernandez-Acenero, A. Ramirez de Molina, R. Barderas, Metabolic reprogramming helps to define different metastatic tropisms in colorectal cancer, Front. Oncol. 12 (2022) 903033, https://doi.org/10.3389/fonc.2022.903033.

[36] R. Linares, S. Tan, C. Gounou, N. Arraud, A.R. Brisson, High-speed centrifugation induces aggregation of extracellular vesicles, J. Extracell. Vesicles 4 (2015) 29509, https://doi.org/10.3402/jev.v4.29509.

[37] C. Gollwitzer, D. Bartczak, H. Goenaga-Infante, V. Kestens, M. Krumrey, C. Minelli, M. Palmai, Y. Ramaye, G. Roebben, A. Sikora, Z. Varga, A comparison of techniques for size measurement of nanoparticles in cell culture medium, Anal. Methods 8 (2016) 5272–5282, https://doi.org/10.1039/C6AY00419A.

[38] R. Rejas-Gonzalez, A. Montero-Calle, A. Valverde, N.P. Salvador, M.J.C. Carballes, E. Ausin-Gonzalez, J. Sanchez-Naves, S. Campuzano, R. Barderas, A. Guzman-Aranguez, Proteomics analyses of small extracellular vesicles of aqueous humor: identification and validation of GAS6 and SPP1 as glaucoma markers, Int. J. Mol. Sci. 25 (13) (2024), https://doi.org/10.3390/ijms25136995.

[39] C. Sbarigia, S. Dinarelli, F. Mura, L. Buccini, F. Vari, D. Passeri, M. Rossi, S. Tacconi, L. Dini, Wild-type and SOD1-g93a SH-SY5Y under oxidative stress: EVs characterization and topographical distribution of budding vesicles, Appl. Nanosci. 4 (2023) 45–60, https://doi.org/10.3390/applnano4010004.

[40] W. Zhang, R. Liu, Y. Chen, M. Wang, J. Du, Crosstalk between oxidative stress and exosomes, Oxid. Med. Cell. Longev. 2022 (2022) 3553617, https://doi.org/10.1155/2022/3553617.

[41] L. Zhu, J. Zang, B. Liu, G. Yu, L. Hao, L. Liu, J. Zhong, Oxidative stress-induced RAC autophagy can improve the HUVEC functions by releasing exosomes, J. Cell. Physiol. 235 (10) (2020) 7392–7409, https://doi.org/10.1002/jcp.29641.

[42] F.J. Romero, M. Diaz-Llopis, M.I. Romero-Gomez, M. Miranda, R. Romero-Wenz, J. Sancho-Pelluz, B. Romero, M. Muriach, J.M. Barcia, Small extracellular vesicles and oxidative pathophysiological mechanisms in retinal degenerative diseases, Int. J. Mol. Sci. 25 (3) (2024), https://doi.org/10.3390/ijms25031618.

[43] W.C. Chang, C.H. Lee, S.H. Chiou, C.C. Liao, C.W. Cheng, Proteomic analysis of aqueous humor proteins in association with cataract risks: diabetes and smoking, J. Clin. Med. 10 (24) (2021), https://doi.org/10.3390/jcm10245731.

[44] G. Velez, D.A. Machlab, P.H. Tang, Y. Sun, S.H. Tsang, A.G. Bassuk, V.B. Mahajan, Proteomic analysis of the human retina reveals region-specific susceptibilities to metabolic-and oxidative stress-related diseases, PLoS One 13 (2) (2018), https://doi.org/10.1371/journal.pone.0193250.

[45] S.H. Lee, J.H. Jung, T.K. Park, C.E. Moon, K. Han, J. Lee, H.K. Lee, Y.W. Ji, C. Y. Kim, Proteome alterations in the aqueous humor reflect structural and functional phenotypes in patients with advanced normal-tension glaucoma, Sci. Rep. 12 (1) (2022) 1221, https://doi.org/10.1038/s41598-022-05273-0.

[46] M.A. Kaeslin, H.E. Killer, C.A. Fuhrer, N. Zeleny, A.R. Huber, A. Neutzner, Changes to the aqueous humor proteome during glaucoma, PLoS One 11 (10) (2016) e0165314, https://doi.org/10.1371/journal.pone.0165314.

[47] S.K. Kodeboyina, T.J. Lee, K. Bollinger, L. Ulrich, D. Bogorad, A. Estes, W. Zhi, S. Sharma, A. Sharma, Aqueous humor proteomic alterations associated with visual field index parameters in glaucoma patients: a pilot study, J. Clin. Med. 10 (6) (2021), https://doi.org/10.3390/jcm10061180.

[48] E.Y. Kang, P.K. Liu, Y.T. Wen, P.M.J. Quinn, S.R. Levi, N.K. Wang, R.K. Tsai, Role of oxidative stress in ocular diseases associated with retinal ganglion cells degeneration, Antioxidants 10 (12) (2021), https://doi.org/10.3390/antiox10121948.

[49] L. Zhang, Z.F. Zhang, Y.N. Hui, F. He, X.R. Guan, J. Zhou, Oxidative stress participates in age-related cataract formation by disrupting connection between lens epithelial cells through c-src/VEGF pathway, Curr. Eye Res. (2023), https://doi.org/10.1080/02713683.2023.2293456.

[50] V.E. Lledó, H.A. Alkozi, J. Sánchez-Naves, M.A. Fernandez-Torres, A. Guzman-Aranguez, Melatonin counteracts oxidative damage in lens by regulation of Nrf2 and NLRP3 inflammasome activity, Exp. Eye Res. 215 (2022) 108912, https://doi.org/10.1016/j.exer.2021.108912.
[51] J. Cabrerizo, J.A. Urcola, E. Vecino, Changes in the lipidomic profile of aqueous humor in open-angle glaucoma, J. Glaucoma 26 (4) (2017) 349–355, https://doi.org/10.1097/IJG.0000000000000603.
[52] F. Anders, J. Teister, S. Funke, N. Pfeiffer, F. Grus, T. Solon, V. Prokosch, Proteomic profiling reveals crucial retinal protein alterations in the early phase of an experimental glaucoma model, Graefes Arch. Clin. Exp. Ophthalmol. 255 (7) (2017) 1395–1407, https://doi.org/10.1007/s00417-017-3678-x.
[53] M. Magharious, P.M. D'Onofrio, A. Hollander, P. Zhu, J. Chen, P.D. Koeberle, Quantitative iTRAQ analysis of retinal ganglion cell degeneration after optic nerve crush, J. Proteome Res. 10 (8) (2011) 3344–3362, https://doi.org/10.1021/pr2004055.
[54] S. Funke, N. Perumal, S. Beck, S. Gabel-Scheurich, C. Schmelter, J. Teister, C. Gerbig, O.W. Gramlich, N. Pfeiffer, F.H. Grus, Glaucoma related proteomic alterations in human retina samples, Sci. Rep. 6 (2016) 29759, https://doi.org/10.1038/srep29759.
[55] L.V. Starostenko, E.A. Maltseva, N.A. Lebedeva, P.E. Pestryakov, O.I. Lavrik, N. I. Rechkunova, Interaction of nucleotide excision repair protein XPC-RAD23B with DNA containing benzo[a]pyrene-derived adduct and apurinic/apyrimidinic site within a cluster, Biochemi. Moscow 81 (3) (2016) 233–241, https://doi.org/10.1134/S0006297916030056.
[56] Z. Wang, S. Zhou, X. Hu, J. Chai, Ginsenosides induce extensive changes in gene expression and inhibit oxidative stress-induced apoptosis in human lens epithelial cells, BMC Complement Med, Therapy 20 (1) (2020) 44, https://doi.org/10.1186/s12906-020-2826-8.
[57] K. Scavelli, A. Chatterjee, D.J. Rhee, Secreted protein acidic and rich in cysteine in ocular tissue, J. Ocul. Pharmacol. Therapeut. 31 (7) (2015) 396–405, https://doi.org/10.1089/jop.2015.0057.
[58] Q. Yan, J.I. Clark, T.N. Wight, E.H. Sage, Alterations in the lens capsule contribute to cataractogenesis in SPARC-null mice, J. Cell Sci. 115 (Pt 13) (2002) 2747–2756, https://doi.org/10.1242/jcs.115.13.2747.
[59] H.Y. Wei, J.L. Liu, B.J. Lv, L. Xing, S.Y. Fu, SPARC modulates expression of extracellular matrix genes in human trabecular meshwork cells, Acta Ophthalmol. 90 (2) (2012) e138–e143, https://doi.org/10.1111/j.1755-3768.2011.02283.x.
[60] T. Liu, L. Xie, J. Ye, Y. Liu, X. He, Screening of candidate genes for primary open angle glaucoma, Mol. Vis. 18 (2012) 2119–2126.
[61] Y. Shiga, K.M. Nishiguchi, Y. Kawai, K. Kojima, K. Sato, K. Fujita, M. Takahashi, K. Omodaka, M. Araie, K. Kashiwagi, M. Aihara, T. Iwata, F. Mabuchi, M. Takamoto, M. Ozaki, K. Kawase, N. Fuse, M. Yamamoto, J. Yasuda, M. Nagasaki, T. Nakazawa, Genetic analysis of Japanese primary open-angle glaucoma patients and clinical characterization of risk alleles near CDKN2B-AS1, SIX6 and GAS7, PLoS One 12 (12) (2017) e0186678, https://doi.org/10.1371/journal.pone.0186678.
[62] D. Skowronska-Krawczyk, L. Zhao, J. Zhu, R.N. Weinreb, G. Cao, J. Luo, K. Flagg, S. Patel, C. Wen, M. Krupa, H. Luo, H. Ouyang, D. Lin, W. Wang, G. Li, Y. Xu, O. Li, C. Chung, E. Yeh, M. Jafari, M. Ai, Z. Zhong, W. Shi, L. Zheng, M. Krawczyk, D. Chen, C. Shi, C. Zin, P.L. Mellon, W. Gao, R. Abagyan, L. Zhang, X. Sun, S. Zhong, Y. Zhuo, M.G. Rosenfeld, Y. Liu, K. Zhang, P16INK4a upregulation mediated by SIX6 defines retinal ganglion cell pathogenesis in glaucoma, Mol. Cell. 59 (6) (2015) 931–940, https://doi.org/10.1016/j.molcel.2015.07.027.
[63] H. Tawarayama, Q. Feng, N. Murayama, N. Suzuki, T. Nakazawa, Cyclin-dependent kinase inhibitor 2b mediates excitotoxicity-induced death of retinal ganglion cells, Invest. Ophthalmol. Vis. Sci. 60 (13) (2019) 4479–4488, https://doi.org/10.1167/iovs.19-27396.
[64] I. Kaur, J. Kaur, K. Sooraj, S. Goswami, R. Saxena, V.S. Chauhan, R. Sihota, Comparative evaluation of the aqueous humor proteome of primary angle closure and primary open angle glaucomas and age-related cataract eyes, Int. Ophthalmol. 39 (1) (2019) 69–104, https://doi.org/10.1007/s10792-017-0791-0.
[65] Y. Tang, Y. Pan, Y. Chen, X. Kong, J. Chen, H. Zhang, G. Tang, J. Wu, X. Sun, Metabolomic profiling of aqueous humor and plasma in primary open angle glaucoma patients points towards novel diagnostic and therapeutic strategy, Front. Pharmacol. 12 (2021) 621146, https://doi.org/10.3389/fphar.2021.621146.
[66] Z. Wang, D. Liu, H. Yuan, A. Li, J. Wang, X. Zhu, W. Xiu, G. Zhang, Y. Chen, L. Chen, X. Xiao, C. He, F. Lu, Association of plasma lactoferrin levels with disease severity in glaucoma patients, Front. Med. 11 (2024) 1385358, https://doi.org/10.3389/fmed.2024.1385358.
[67] T. Yabana, K. Sato, Y. Shiga, N. Himori, K. Omodaka, T. Nakazawa, The relationship between glutathione levels in leukocytes and ocular clinical parameters in glaucoma, PLoS One 14 (12) (2019) e0227078, https://doi.org/10.1371/journal.pone.0227078.
[68] B. Can Demirdogen, S. Demirkaya-Budak, G. Ozge, T. Mumcuoglu, Evaluation of tear fluid and aqueous humor concentration of clusterin as biomarkers for early diagnosis of pseudoexfoliation syndrome and pseudoexfoliative glaucoma, Curr. Eye Res. 45 (7) (2020) 805–813, https://doi.org/10.1080/02713683.2019.1698055.
[69] H. Gonzalez-Iglesias, L. Alvarez, M. Garcia, J. Escribano, P.P. Rodriguez-Calvo, L. Fernandez-Vega, M. Coca-Prados, Comparative proteomic study in serum of patients with primary open-angle glaucoma and pseudoexfoliation glaucoma, J. Proteonomics 98 (2014) 65–78, https://doi.org/10.1016/j.jprot.2013.12.006.
[70] V.M. Beutgen, N. Perumal, N. Pfeiffer, F.H. Grus, Autoantibody biomarker discovery in primary open angle glaucoma using serological proteome analysis (SERPA), Front. Immunol. 10 (2019) 381, https://doi.org/10.3389/fimmu.2019.00381.
[71] N. Nezu, Y. Usui, A. Saito, H. Shimizu, M. Asakage, N. Yamakawa, K. Tsubota, Y. Wakabayashi, A. Narimatsu, K. Umazume, K. Maruyama, M. Sugimoto, M. Kuroda, H. Goto, Machine learning approach for intraocular disease prediction based on aqueous humor immune mediator profiles, Ophthalmology 128 (8) (2021) 1197–1208, https://doi.org/10.1016/j.ophtha.2021.01.019.
[72] I. Hecht, A. Achiron, L. Ben Haim, V. Sorin, M. Mimouni, I. Kaiserman, Refractive surgery in the late adulthood and adolescent age groups, Graefes Arch. Clin. Exp. Ophthalmol. 257 (9) (2019) 2057–2063, https://doi.org/10.1007/s00417-019-04396-x.